JOURNAL OF MATERIALS SCIENCE **40** (2005) 263–283

Preparation of alumina films by the sol-gel method

Y. KOBAYASHI*,‡, T. ISHIZAKA§, Y. KUROKAWA§
Department of ‡Chemical Engineering and §Material Chemistry, Graduate School of Engineering, Tohoku University, Aoba, Aramaki-aza, Aoba-ku, Sendai 980-8579, Japan
E-mail: yoshio@mickey.che.tohoku.ac.jp

This review describes our study on preparation of alumina films by a sol-gel process and their several applications that have been investigated since 1986. Alumina films were prepared from alkoxide or inorganic salt. Both as-prepared alumina films were transparent in ultraviolet, visible and near infrared regions. The alumina from inorganic salt (inorganic alumina) was structureless even after annealed at 300–700°C in air, while the alumina from alkoxide (alkoxide alumina) was in pseudo-boehmite at an annealing temperature lower than 400°C and was in γ- or δ-type at 400–700°C. Both alumina films became opaque after annealed at temperatures above 1000°C. The inorganic alumina film annealed at 800°C showed a gas permeability that was influenced by physico-chemical properties of penetrant and alumina. Composite films of alumina and poly(vinyl alcohol) (PVA) were hydrophilic but insoluble in water, and removal of PVA from the composite films by annealing at 600°C led to formation of transparent alumina films. Such properties enabled us to use a counter diffusion method for fabricating γ-Fe_2O_3-doped alumina films. Alumina films doped with organic dyes such as laser dyes, hole-burning dyes and non-linear optical dyes, which were fabricated by gelation of dye-added alumina sol, exhibited laser emission, hole-spectra and second- or third-harmonic generation properties, respectively. Hydrogenation of alkene was catalyzed by Ni nanoparticles doped alumina films that were prepared by gelation of Ni^{2+} solution-added alumina sol and annealing the Ni^{2+}-doped alumina gel in hydrogen gas. Nonlinear optical properties were observed for alumina films doped with CdS, Au and Ag nanoparticles, which were fabricated by gelation of Cd^{2+}, $HAuCl_4$ and $AgNO_3$ solution-added alumina sols and annealing the Cd^{2+}-doped alumina gel in H_2S gas and the Ag^+- and Au^{3+}-doped alumina gels in H_2 gas. Rare earth metal ion-doped alumina films, which were prepared by gelation of rare earth metal ion solution-added alumina sol and annealed the ion-doped alumina gel, exhibited not only normal luminescence but also up-conversion emission, energy transfer type luminescence and long lasting luminescence.

1. Introduction

A sol-gel method has been drawn much interest in recent years and is now being widely used to prepare ceramic materials [1–6]. Metal alkoxides, e.g., tetraethyl orthosilicate, are hydrolyzed and polymerized in the presence of catalyst such as hydrochloric acid, nitric acid acetic acid or ammonia as described by Equations 1 and 2:

$$Si(OC_2H_5)_4 + 4H_2O \rightarrow Si(OH)_4 + 4C_2H_5OH \quad (1)$$

$$Si(OH)_4 \rightarrow SiO_2 + 2H_2O \quad (2)$$

These reactions are dependent on various conditions, i.e., temperature and concentrations of alkoxide, water and catalyst.

The fascinating features of the sol-gel technique are (1) room temperature or slightly elevated temperature (<100°C) gel formation, (2) easily varied compositions, (3) comparably high purity and (4) low sintering temperature. Such materials by the sol-gel technique have been applied for gas separation, coating film, fiber, catalysis, optics, electronics, etc. [1–6].

Many works are concerned with silica derived from silicone alkoxide. However, other metal oxides have not so intensively studied as silica. From this kind of view, we have been studying on alumina since 1986 [7–42]. In this review, we introduce preparation of alumina films by sol-gel method and their various applications for coating on substrate, gas separations, magnetism, catalysis, thin-film laser emission, hole-burning, nonlinear optics and high quality luminescence.

*Author to whom all correspondence should be addressed.

2. Alumina films

2.1. Introduction

Alumina films can be prepared mainly by two sol-gel methods. One uses aluminum alkoxide as a starting reagent, which was performed by Yoldas [43]. The alkoxide route to ceramics has been described in several areas [1–6]. Typically, aluminum alkoxides are useful compounds for preparing alumina sol and alumina film by the sol-gel process. The other method we proposed [7] uses aluminum inorganic salt as a starting reagent. The majority of works on the sol-gel process has dealt with alkoxides as precursors. In contrary, gel films also can be prepared with aqueous sol-gel process. However, it appears that the aqueous process is relatively limited. Materials formed from aqueous sol are not as pure as that from alkoxide. The aqueous process is readily available and is inexpensive. In this section, we introduce and compare both two methods.

2.2. Alumina films derived from alkoxide

2.2.1. Preparation and structural characterizations

Yoldas prepared a transparent alumina sol by hydrolyzing aluminum triisopropoxide with water [43]. After heating a mixture of the alkoxide and water at 80°C under stirring for 1 h, the mixture became slurry. Then, acid was added to this slurry as a peptizing agent. Typically, a molar ratio of water, alkoxide and acetic acid was 100:1:0.15. In 8 h, the slurry became a transparent sol. In peptization, the type of acid plays a much more important role than the controlling pH of the solution. Here, two types of acids of hydrochloric acid and acetic acid were employed [8, 16]. In the HCl system, a clear sol was obtained at a molar ratio of HCl to alkoxide of 0.06 and its transmittance decreased above 0.06 mol. In the acetic acid system, the transparency of a sol increased with an increase in a molar ratio up to about 0.15, and the transparency gradually decreased above a molar ratio of 0.15. Hence, acetic acid was chosen to obtain a clear sol.

The sol was transferred into a petri dish and was allowed under atmosphere to give a transparent gel film by dehydration. In this review, the transparent gel film is called "alkoxide alumina film" or simply "alkoxide film." The transparent alkoxide alumina film was peeled off from the dish after the formation of the gel film. Transmittance data of the alkoxide film treated at various temperatures are given in Fig. 1a [26, 33]. The alkoxide film was transparent even after annealed 600°C. This high transmittance was given up to 800°C and the alkoxide film became gradually opaque with an increase in an annealing temperature (not shown), accompanying formation of α-alumina. XRD patterns are shown in Fig. 2a [26, 33]. Peak positions for the alkoxide film annealed at a temperature lower than 300°C were due to those of boehmite. At 400°C, patterns of both pseudoboehmite and γ-alumina were observed. Annealing the alkoxide films at 600–1000°C resulted in appearance of a peak that corresponded to γ-type

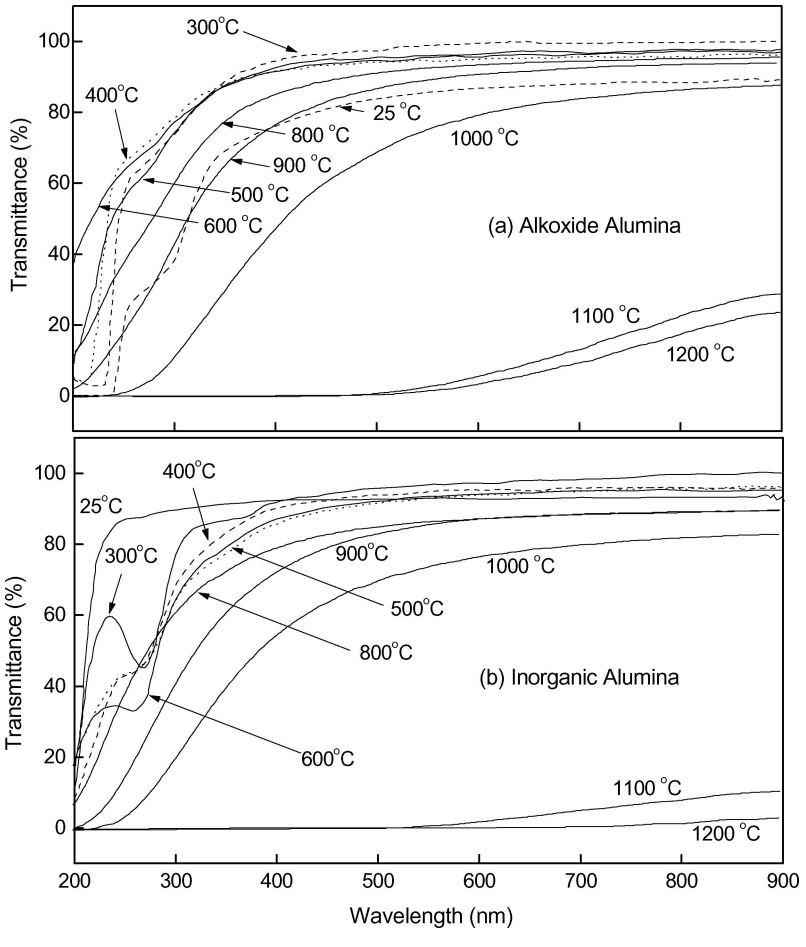

Figure 1 Transmittance of alkoxide alumina films annealed at various temperatures. The thickness of each film was around 100 μm.

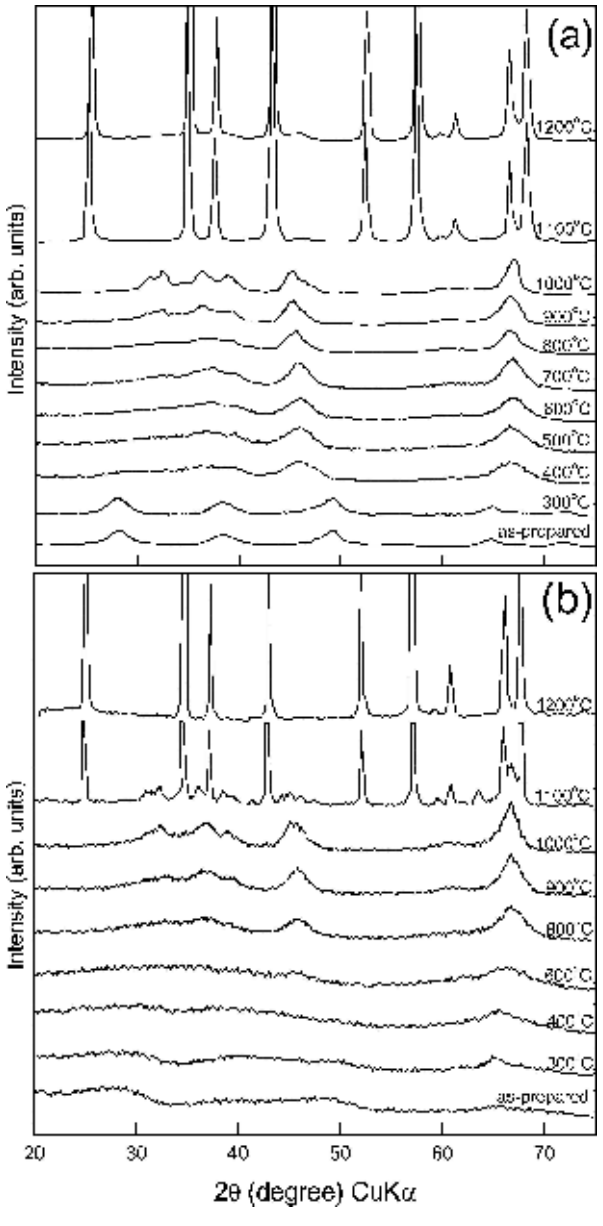

Figure 2 XRD patterns of (a) alkoxide and (b) inorganic alumina films annealed at various temperatures. Reprinted from *J. Appl. Phys.* **90** (2001) 243.

alumina. The alkoxide films annealed at temperatures above 1000°C became white and α-alumina.

2.2.2. Gas separation

Gas separation by membrane has been suggested as an alternative to distillation methods. Membranes may be divided into homogeneous and microporous types or organic polymer and inorganic types. There are many reports on organic polymer membranes for the gas separation. However, there are a few reports on inorganic membranes, exclusively on a porous glass membrane [44, 45]. The use of inorganic membranes is advantageous if they are used at high temperature. Since it is difficult to obtain a crack-free inorganic membrane because of fragility, not much information has been published on gas permeability of inorganic membranes at the moment. Gas permeability of the alkoxide alumina films to various gases was intensively investigated in our previous works [8, 9]. According to thermogravimetric curve [8], pyrolysis was completed at an annealing temperature of 600°C. The gas permeability was examined for the film annealed at 800°C. A pore size roughly calculated by applying the Kelvin equation for the isotherms of nitrogen was 2.5–3.5 nm [8, 9]. Fig. 3 shows permeability coefficient as a function of molecular weight. Group I, II, III and IV stand for permanent, aliphatic hydrocarbon, aromatic hydrocarbon and polar gases, respectively. In the group I, the permeability decreased approximately linearly with an increase in square root of molecular weight, which indicated the gases with small molecular weight flew through pores of the alumina according to Knudsen flow. For the gases with large molecular weight, it appeared that the permeability behaved as expected for viscous flow. For group II penetrants, permeability of normal chain hydrocarbon gasses increased with an increase in molecular weight, in the range of molecular weights smaller than C_6. Probably, the gas flows were mainly governed by viscous flow. Permeabilities of isomers were lower than those of the normal chain hydrocarbon gasses, and in the range of molecular weights larger than C_6, permeability of normal chain hydrocarbon gasses decreased with an increase in molecular weight. Hindrance effects probably acted on the permeabilities of branched and larger penetrants. For the group III, the permeability decreased with the number of $-CH_3$ group, since branching plays an important role in permeability. For the group IV, permeabilities were lower than other groups because of strong interaction between penetrant and alumina.

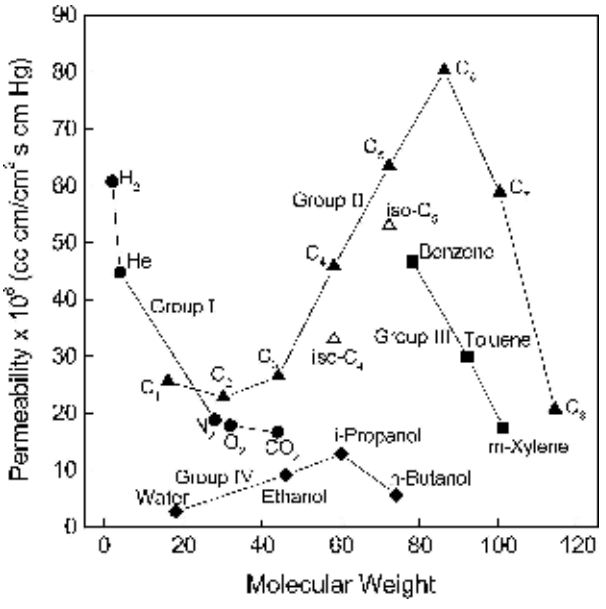

Figure 3 Apparent permeabilities of various gases at 20°C through alkoxide alumina membrane annealed at 800°C. Group I–IV stand for permanent gases, aliphatic gases, benzenes with methyl groups and alcohols. Originated from *J. Non-Cryst. Sol.* **94** (1987) 160.

2.3. Alumina films derived from inorganic salt

2.3.1. Preparation and structural characterizations

Transparent alumina films also can be prepared from an aqueous sol derived by hydrolyzing aqueous

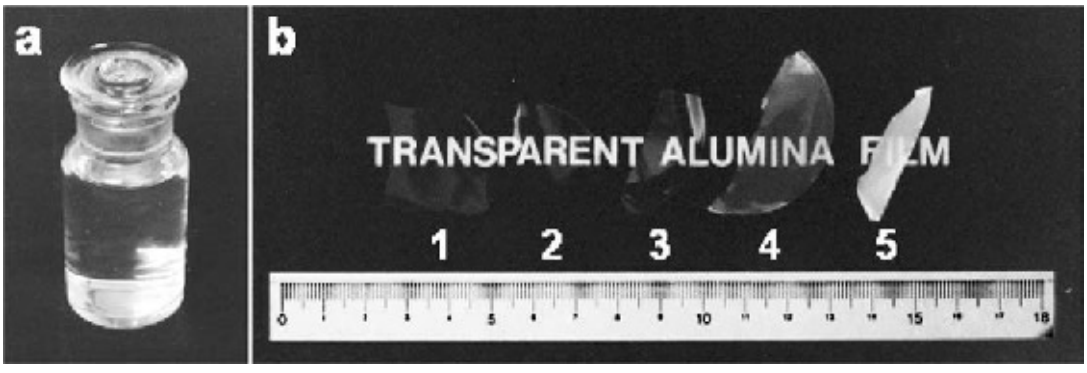

Figure 4 Photographs of (a) inorganic alumina sol and (b) alumina films annealed at (1) 25°C (as-prepared), (2) 600°C, (3) 800°C, (4) 1000°C, and (5) 1200°C.

$AlCl_3 \cdot 6H_2O$ [7]. A 6 M aqueous NH_3 solution was used to precipitate hydrous aluminum hydroxide from a 0.2 M aqueous $AlCl_3$ solution. The precipitated hydroxide was then aged for 12 h, filtered and washed with pure water. Peptizing the cleaned precipitate with acetic acid under reflux at 80°C for 8 h led to formation of a viscous transparent sol, in which the molar ratio of acetic acid to $AlCl_3 \cdot 6H_2O$ was 0.15. A photograph of the obtained alumina sol shown in Fig. 4 revealed a transparent sol. The acid addition alone did not bring about the peptization; the heat treatment significantly enhanced the peptization rate [7]. Fig. 5 shows a TEM image of alumina sol particles [7]. Ultrafine particles with the size of about 10 nm were observed, which might be attributed to hydrous and amorphous polynuclear species. According to a dynamic light scattering measurement [18], the sol dispersed particle sizes with sizes of 30–50 nm. Aggregate particles composed of the 10 nm-sized particles were probably detected with the scattering measurement.

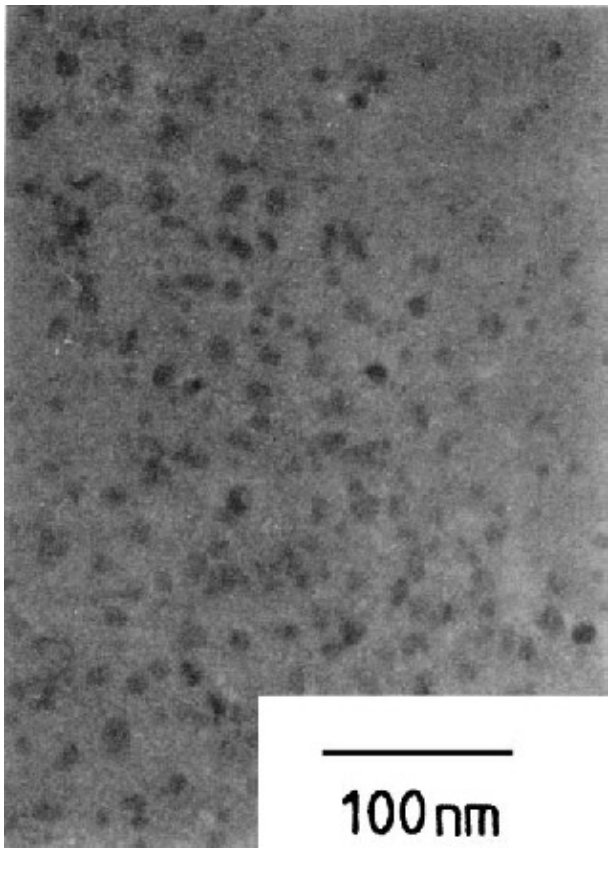

Figure 5 TEM image of particles in inorganic alumina sol. Reprinted from *J. Mater. Sci. Lett.* **5** (1986) 1070.

Removal of water from the sol solution yielded a viscous sol as well as the alkoxide alumina sol. By further removal, the sol was finally transformed into a transparent gel film on a petri dish (Fig. 4). In this review, the gel film derived from inorganic salt is called "inorganic alumina film." To monitor the hydrolysis of a sol-gel transformation, organic dyes such as pyranine and 7-azaindole were incorporated into the alumina sol [15, 18]. Pyranine has fluorescence peaks at 440 nm for an acidic for and 550 nm for a basic form, respectively. 7-Azaindole has fluorescence that is sensitive to the microenvironment around the dye molecules. From fluorescence measurements of these dyes during the dehydration process, the sol-gel transition took place remarkably when about 85 wt% of water was removed from the sol.

Figs 4, 1b and 2b show a photograph, transmittance data [7, 21, 26, 33, 36] and XRD patterns [7, 21, 26, 33, 36] of the inorganic alumina films annealed at various temperatures. The inorganic alumina film was transparent even after annealed at 1000°C. Above 1000°C, the film became gradually opaque with an increase in annealing temperature because of formation of α-alumina. As well as the alkoxide alumina, the inorganic alumina gave high transmittance in the ultraviolet and visible ranges. Reflection positions of as-prepared inorganic alumina (25°C) were probably assigned to pseudoboehmite or poorly crystallized boehmite. The inorganic aluminas annealed at 300–800°C appeared to be more or less structureless compared to the alkoxide alumina, although it seemed to partially contain γ-alumina. It is known that thermal transitions are affected by kinds of starting materials, coarseness of particles and impurities. This is probably the reason the difference between the alkoxide and inorganic aluminas was observed. Annealing at 1100°C resulted in appearance of diffuse lines that corresponded to θ-alumina. In summary, the transition of crystalline phase took place as follows: δ (800°C), $\theta + \alpha$ (1100°C), α (1200°C).

Alkoxide alumina shows an emission peak at 420–450 nm that is associated with these centers that are attributed to carbon formation (organic residue) and/or five co-ordinate state of aluminum [46]. For the

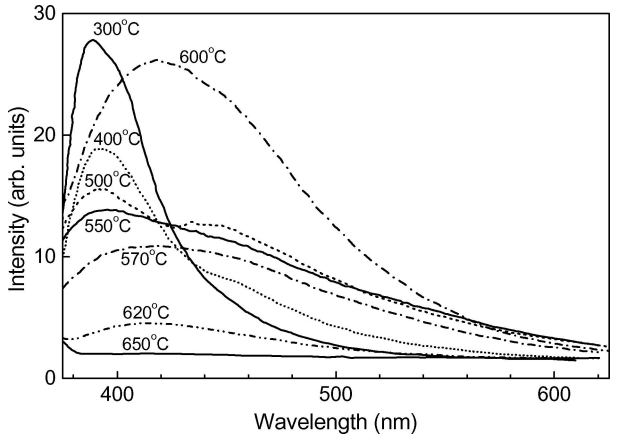

Figure 6 Luminescence spectra of inorganic alumina films annealed at various temperatures. Reprinted from *J. Mater. Sci. Lett.* **17** (1998) 275.

inorganic alumina films, luminescence was also observed, as shown in Fig. 6 [33, 36]. The inorganic alumina exhibited stronger luminescence than the alkoxide alumina [33, 36]. For amorphous SiO_2, one of common defects is a center with an optical absorption band, the so-called E′-centre [47, 48]. The inorganic alumina was probably amorphous and in a state similar to so-called "glass" compared to the alkoxide alumina. A luminescence peak was observed at 390 nm for the 300°C-annealed inorganic alumina. Above 300°C, the peak intensity at 390 nm was reduced and then a new emission band appeared at 430 nm. This emission was the strongest at 600°C and vanished above 600°C. Annealing temperature, at which the emission at 430 nm appeared, seemed to correspond approximately to annealing temperature for the γ-alumina formation. Solid state NMR has been developed to obtain more insight into microstructure, though amorphous states are difficult to be characterized adequately by XRD. Many NMR studies have been performed on alumina sol and gel [49–52]. Fig. 7 shows ^{27}Al MAS NMR for inorganic alumina. Besides the resonance lines attributable to tetrahedrally (Al^{IV}) and octahedrally (Al^{VI}) co-ordinated aluminum, a line that could be assigned to petahedrally (Al^{V}) co-ordinated aluminum was observed for the inorganic alumina. The Al^{V} peak intensity changed slightly with treatment temperature. The peak height corresponded roughly with the luminescence intensity at 430 nm. However, that correspondence was not enough, i.e., luminescence was not observed at 430 nm though an Al^{V} peak was detected for the inorganic alumina treated at 700°C. This indicated that luminescence centers were limited to special defect sites that had appropriate depth defects. EPR (electron paramagnetic resonance) spectra for the inorganic alumina annealed at various temperatures were also measured (not shown) [41]. The observed signals for the inorganic alumina annealed at 300, 500 and 800°C was ascribed to an electron trapped at oxygen vacancy associated with Al^{V}. The signal intensities for the alumina annealed at 300 and 500°C were intense, and that at 800°C was very weak. This result suggested that Al^{V} was one of the emission centers.

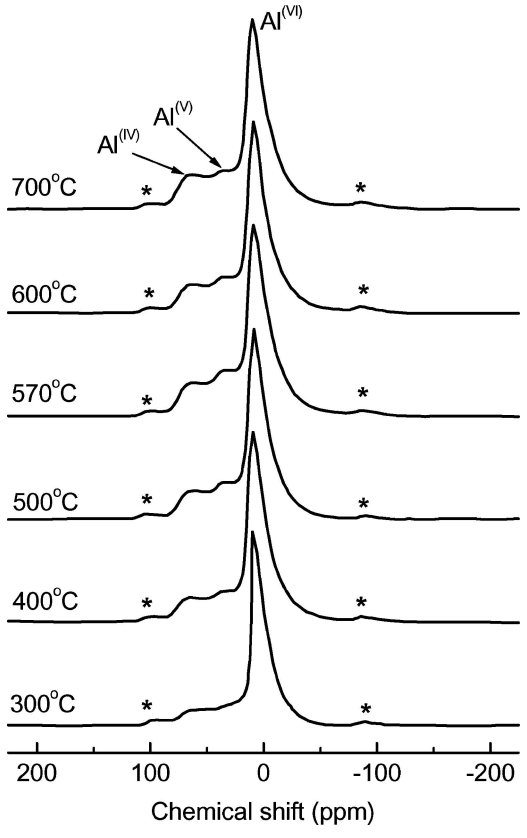

Figure 7 ^{27}Al MAS NMR for inorganic alumina annealed at various temperatures. Reprinted from *J. Mater. Sci. Lett.* **17** (1998) 275.

2.3.2. Coating

The sol-gel method is a suitable technique for coating a substrate. Coatings performed by the sol-gel method can protect against oxidation or corrosion to acids, act as insulators, or enhance the scratch resistance of the substrate. Because of a variety of applications, the sol-gel method has been extensively investigated [53]. For example, the SiO_2-coating of substrates has been well studied and applied [54, 55]. There have been numerous studies on thin alumina coatings using sol derived from alkoxide [56–58], but only a few studies have been reported on the thick alumina coating that is sometimes used on substrates [59]. A thick alumina coating on quartz glass and nickel substrates were performed using the inorganic alumina sol by a dipping method [42]. Vickers hardness of the alumina coated quartz glass increased with an increase in annealing temperature, and the Vickers hardness for the 800°C-annealed sample was as large as 550 kgw/mm^2. SIMS (secondary ion mass spectrometry) depth profiles for alumina-coated quartz glass plates annealed at various temperatures are shown in Fig. 8. The diffusion of alumina into the surface took place in conjunction with an increase in annealing temperature and annealing time. Thus, complex metal oxide was probably formed in the diffusion layer, and the formation of this layer induced an increase in the adhesiveness of alumina on the substrate. It can be considered that the formation of the complex metal oxide between the alumina film and the quartz glass plate generated such a large hardness. Similar results were also obtained for the Ni substrate.

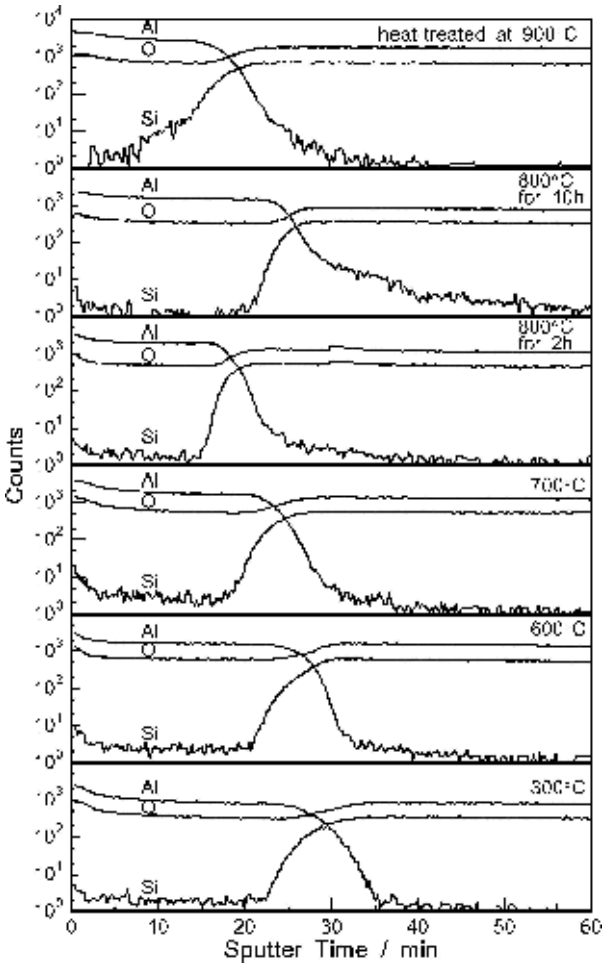

Figure 8 SIMS depth profiles for inorganic alumina coated quartz glass substrates annealed at 300, 600, 700, 800 and 900°C. Sputtering was performed using a Cs^+ ion beam. Etching rate was 0.05–0.15 μm/h. Reprinted from *J. Mater. Sci.* **38** (2003) 1239.

3. Alumina-polymer composite films

3.1. Introduction

There are many investigations on treatment of inorganic oxide particles or clay with organic polymer materials in heterogeneous system [60, 61]. In this system, micron-sized particles are used. Fine particles are suitable for being dispersed into organic material, i.e., polymer, with a view to obtaining a more homogeneous composite. A candidate way to obtain a homogeneous composite would be to use the sol-gel method [62]. In this section, we introduce a preparation method of alumina-polymer composite films and their application.

3.2. Preparation of alumina-polymer composite films

Poly(vinyl alcohol) (PVA) was used as a polymer for composite, since PVA was water-soluble and thereby it was possible to homogeneously mix alumina sol with aqueous PVA. Mixture of the alkoxide alumina sol and the aqueous PVA was poured into a petri dish and converted to a gel by drying in atmosphere. PVA contents were 0–100 wt% for the composite film. The composite gel films were transparent at all the PVA concentrations. A photograph of PVA-alumina composite film is shown in Fig. 9 [16]. The composite films containing PVA below 20 wt% were brittle and difficult to be molded into membrane. Above 70 wt%, the composite films became flexible and easily molded. Removal of PVA from the composite films by annealing at 600°C in air made the obtained films fragile and lost their original forms. The composite films containing 40–50 wt% PVA kept their original forms and transparency even after annealed at 600°C in air. The composite film containing 50 wt% PVA could be drawn up to five times initial length in saturated vapor of water at 25°C, and the drawn-up film was still transparent. According to X-ray diffraction pattern, the boehmite structure of alumina, which was originally oriented to the film plane, became more oriented by drawing. After annealed at 600°C in air, the composite film kept its original form. However, the film became partially white because of some wrinkles and influence of light scattering.

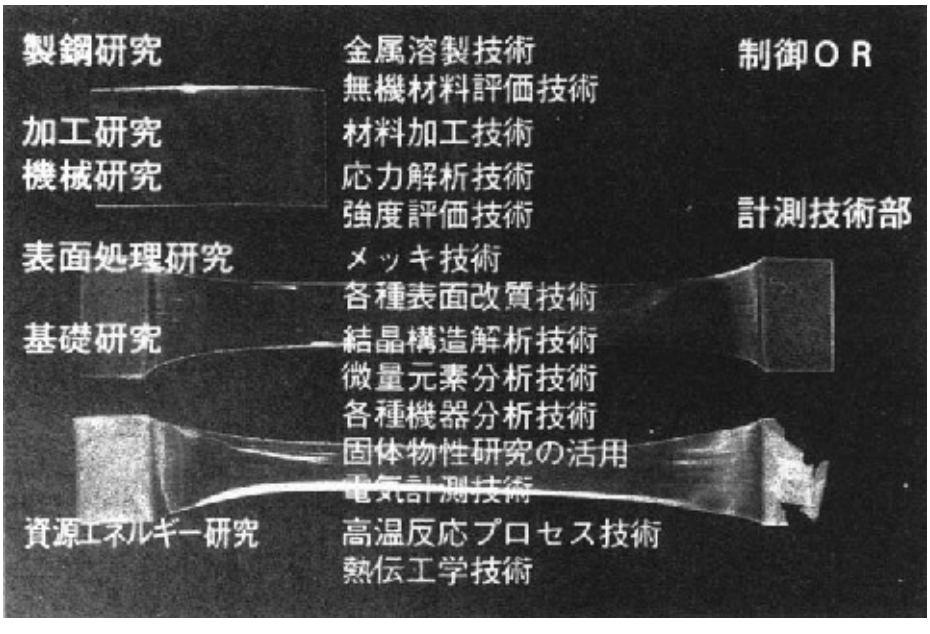

Figure 9 Photographs of composite membranes: as-cast membrane (top), as-draw membrane (middle), calcination residue of as-draw membrane (bottom). PVA: alumina = 1:1 by weight. Reprinted from *J. Appl. Polym. Sci.* **39** (1990) 371.

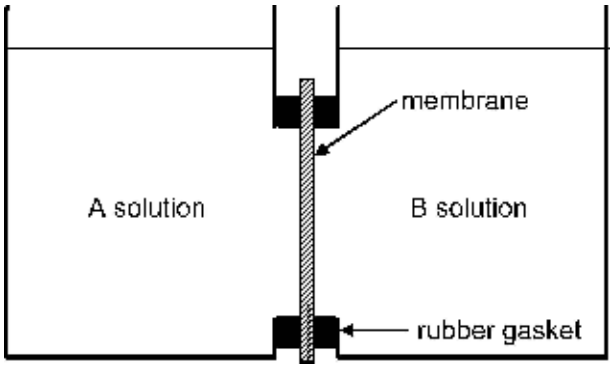

Figure 10 Schematic diagram of the counter diffusion apparatus.

3.3. Preparation of γ-Fe_2O_3/alumina films by a counter diffusion method

Kurokawa proposed a "counter diffusion method", which allows the dispersion of various types of fine particles in a film matrix [63]. Fig. 10 shows a schematic diagram of the counter diffusion apparatus, which has two containers separated by a film. Assuming that compound *A* reacts with compound *B* to be precipitate of compound *C*, fine particles of compound *C* are produced in the film. Their particle size can be varied with pore size of the membrane. Nanoparticles of iron oxide, Ni, Ag, and CdS were successfully incorporated into cellulose acetate films and cross-linked PVA films with the method, and their properties such as catalysis, magnetics, optics and surface enhanced Raman spectroscopy were investigated [25, 64–82]. The counter diffusion method requires the film matrix to be hydrophilic but insoluble in water, when aqueous solutions are used as reactant solutions. Therefore, organic polymers such as cellulose acetate and cross-linked PVA were used as film matrix in this method. The 50 wt% PVA-alumina composite film revealed hydrophilicity and insolublity in water after heated at 100°C. Therefore, the 50 wt% PVA-alumina composite film heated at 100°C was used as a matrix for the counter diffusion method. Then, we attempted to disperse iron hydroxide fine particles into the composite film by using the counter diffusion method [81]. Aqueous $Fe(NO_3)_3$ and aqueous NaOH were placed into the respective containers, as shown in Fig. 10. Fe^{3+} and OH^- ions diffused counter-currently and contacted inside of the film, and consequently $Fe_2O_3 \cdot nH_2O$ precipitates were produced in the film, as seen in inset of Fig. 11.

In the Section 3.2, it was shown that the transparent alumina films were fabricated by annealing the PVA-alumina composite films at 600°C. For the PVA-alumina films containing iron hydroxide, brown films were obtained by annealing the films at 600°C in air. According to the XRD analysis, $Fe_2O_3 \cdot nH_2O$ was transformed to nanometer-sized γ-Fe_2O_3 particles. The Fe_2O_3 contents increased up to about 25 wt% with an increase in the reaction time. Fig. 11 shows the magnetization curve for the Fe_2O_3-alumina film. The film set parallel to the magnetic field had a steeper slope in the portion of the initial magnetization range than did the perpendicular one, which indicated that the film was easier to magnetize parallel to the film plane. In other words, the Fe_2O_3-alumina film enhanced a magnetic anisotropy. The alumina structure in the PVA-alumina composite film has a preferred orientation parallel to the film plane. This orientation probably controlled the crystal growth direction of $Fe_2O_3 \cdot nH_2O$, and thereby, the crystal growth direction of the γ-Fe_2O_3 fine particles became parallel to the film plane.

4. Organic dye-doped alumina films

4.1. Introduction

One application of the ability to trap organic dye in a matrix is for optical materials. One of the key problems in the application is the matrix that hosts the dye. Organic network in an organic matrix is more flexible than the inorganic one. This allows greater rotational and translational freedom in the organic matrix compared with an inorganic matrix. This results in a lowering of the photochemical efficiency. Moreover, the organic matrix is inferior to the inorganic matrix because the former is photochemically and thermally unstable. The sol-gel process for preparing inorganic oxide glass has been studied by many researchers. Avnir *et al.* [83–85], Fujii *et al.* [86], Makishima and Tani [87] and Dunn and Zink [88] reported that organic dyes could be doped in a silica glass by the sol-gel process. However, there are few reports on alumina films as a host for organic dyes. In this section, we introduce preparation of organic dye-doped alumina films and their application for optical materials.

4.2. Laser emission

A conventional dye laser system is big and difficult to deal with. If a film- or fiber-type dye laser becomes usable, the laser system would be small and light, and easier to deal with. Several studies on laser emissions of films doped with laser dyes have been reported. The authors prepared alumina films doped with laser dyes and researched their emission properties [15, 18, 24]. The inorganic alumina sol was mixed with dye solution. The mixture was converted into a gel film by slow dehydration in air. Next, the gel film was dried in a dry box at 100°C in for 2 h. During the gelation, the dye molecules were trapped in the alumina matrix. Fig. 12 shows a photograph of dye-doped inorganic alumina films. No aggregates were observed by naked eyes. The laser dye-doped films were pumped transversely by a pulsed N_2 laser (peak power 100 kW, pulse width 5 ns, repeat cycle 1 pulse/s) focused through a cylindrical lens. The characteristics of laser output from an edge of the film were measured at 90° to the excitation N_2 laser beam using a monochromator and a phototube oscilloscope. Fig. 13 shows absorption and fluorescence spectra of rhodamine 6G (R6G). Two bands were observed in absorption spectra. According to the literature [89, 83], the longer wavelength band was due to monomeric molecules and the shorter wavelength band to dimers. These band positions of R6G in alumina red-shifted compared with those in aqueous

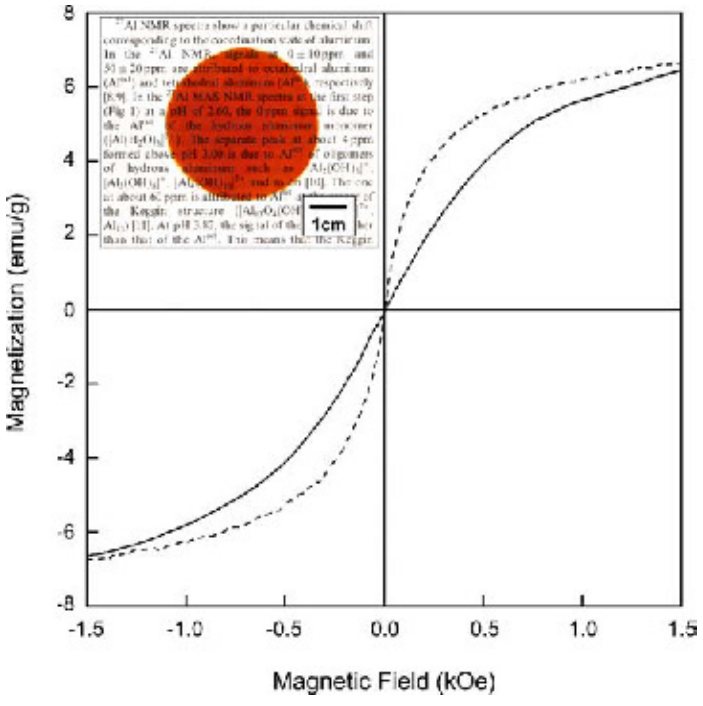

Figure 11 Magnetization curves of Fe_2O_3-doped alkoxide alumina film with a dopant time of 6 h. Magnetic fields were perpendicular (solid line and parallel (dotted line) to the film plane. Reprinted from *Chem. Mater.* **9** (1997) 1887. Inset shows photograph of PVA-alkoxide alumina composite film embedded with iron hydroxide by a counter diffusion method.

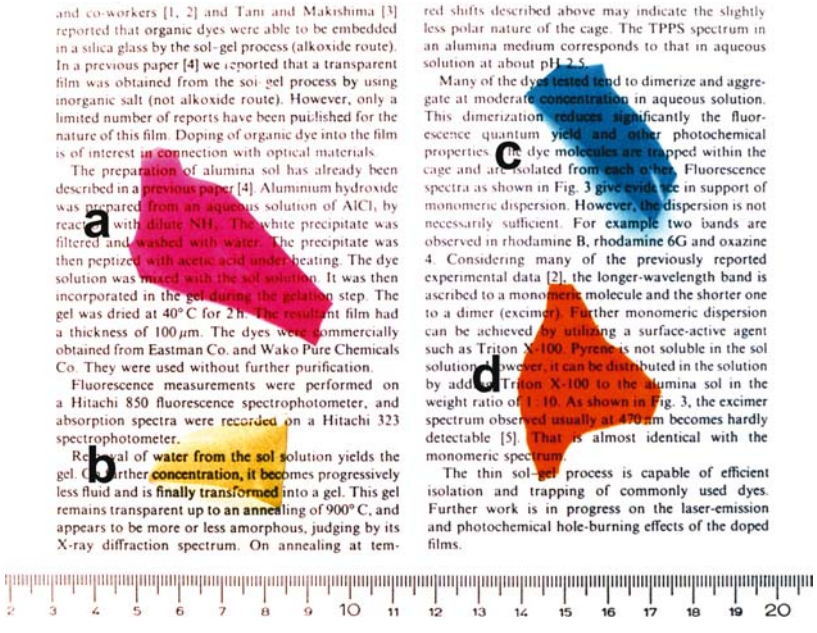

Figure 12 Photographs of inorganic alumina films incorporated with (a) rhodamine 6G, (b) α, β, γ, δ-tetrakis (4-sulfophenyl) porphine, (c) tetrasulfophthalocyanine and (d) CdS.

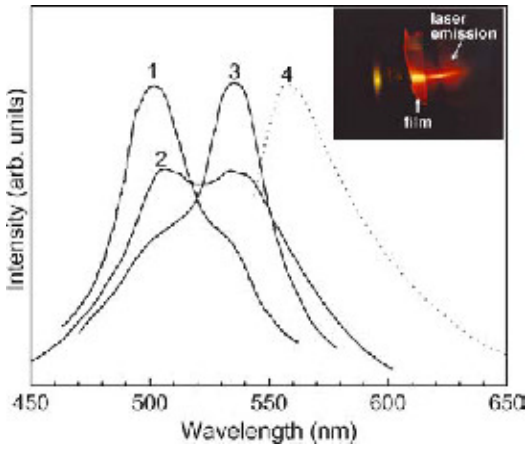

solution, which indicated that local environment of alumina matrix around R6G was slightly less polar than water [83, 84]. This R6G-doped alumina exhibited no laser emission. Dye aggregation such as dye

Figure 13 Absorption and fluorescence spectra of rhodamine 6G. (1) Absorption spectrum in water; (2) Absorption spectrum in inorganic alumina; (3) Absorption spectrum in alumina containing 10 wt% of Triton X-100; (4) Fluorescence spectrum ($\lambda_{ex} = 530$ nm) in alumina. The dye concentrations are 10^{-2} M. Reprinted from *J. Non-Cryst. Sol.* **105** (1988) 198. Inset shows photograph of laser light emitted from inorganic alumina film doped with rhodamine 6G. Pumping N_2 laser was introduced to the film with an incident angle of 90° for the film. Reprinted from *Zairyo Gijutsu* **11** (1993) 197.

dimerization is the basic cause for concentration quenching of dye fluorescence. In aqueous solutions, the band due to dimers was clearly observed at shorter wavelength. The dimer band was largely reduced in the alumina film. However, the reduction of dye aggregation seemed not to be sufficient for laser emission. A complete monomeric dispersion could be achieved by an addition of a surfactant, Triton X-100, to the aqueous R6G solution, as shown in Fig. 13 [12]. This R6G-doped alumina containing Triton X-100 gave a laser emission, as shown in inset of Fig. 13. Conversion efficiency was estimated 2.1% from the characteristics of output power as a function of the pumping power. This value was close to that measured in a plastic film. The N_2 laser-irradiation reduced the R6G laser output power because of dye bleaching. Logarizm of the R6G laser output power decreased proportionally with an increase in shot number of pumping pulse, which indicated that the laser emission was generated with a one-photon process. This photo-bleaching was prevented by addition of β-cyclodextrin [20], since R6G dye molecules are trapped into a ring of β-cyclodextrin and then are protected against O_2 molecules. Besides R6G, alumina film doped with rhodamine B (RB), sulforhodamine 101, coumarin 1 (C1) and 1,2-(1-naphthyl)-5-phenyloxazole (α-NPO) also exhibited laser emission.

The N_2 laser is used as a convenient pump for a wide variety of dye lasers. However, it is difficult to pump laser dyes with the N_2 laser, if their absorption coefficients of dyes at a wavelength of N_2 laser (337 nm) and/or their fluorescence quantum efficiencies for N_2 laser pumping are too low. This problem has been solved by addition of energy donor dyes with a net absorption at a wavelength of an exciting laser [90]. Furthermore, according to Förster-Dexter theory, the fluorescence of the donor must overlap an absorption band of the acceptor, thereby allowing an efficient energy transfer of the excitation from the donor to the acceptor dyes. The alumina film was doped with 2,5-diphenyloxazole (PPO) and α-NPO in the presence of cetyl trimetylammonium bromide (CTAB). CTAB was suitable for monomeric dispersion of PPO and α-NPO molecules in the film, compared with Triton X-100. Fig. 14 shows absorption and fluorescence spectra of the alumina films doped with PPO and α-NPO [24]. In comparison, spectra of the alumina film doped with PPO or α-NPO alone are also shown. The absorption spectrum of the PPO-α-NPO-doped film appeared a sum of the spectra of PPO and α-NPO. In contrary, a fluorescence peak position of both dyes-doped film corresponded to that of α-NPO. The PPO-α-NPO-doped film gave laser emission at about 400 nm by N_2 laser irradiation. Energy transfer probably took place from PPO to α-NPO, since that laser emission wavelength, 400 nm, corresponded to the fluorescence peak position of α-NPO. Fig. 15 shows an effect of PPO concentration on the emitted laser power [24]. The laser power increased with an increase in the PPO concentration up to 3.5×10^{-2} M. A five or more fold increase in the emission power was obtained, relative to the emission at PPO concentration of 1×10^{-2} M. However, the laser emission power decreased with an increase in the

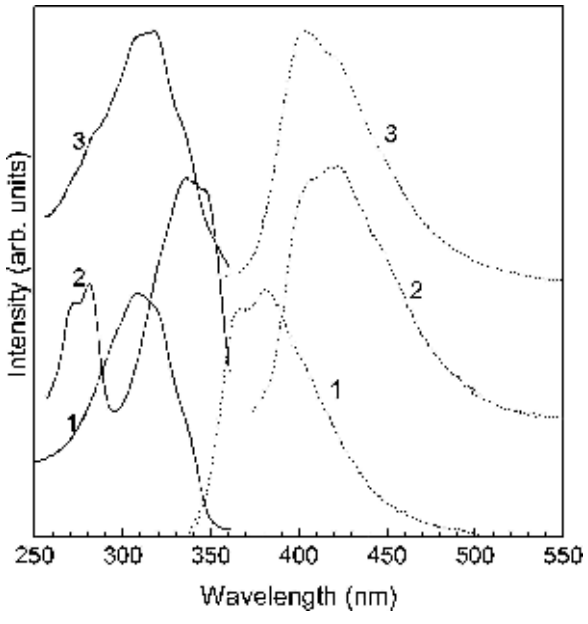

Figure 14 Absorption (solid lines) and fluorescence (dotted lines) spectra of inorganic alumina films doped with laser dye. Samples are alumina films doped with (1) PPO, (2) α-NPO and (3) both PPO and α-NPO. Each film contains 10 wt% of CTAB. Reprinted from *Nippon Kagaku Kaishi* (1992) 1257.

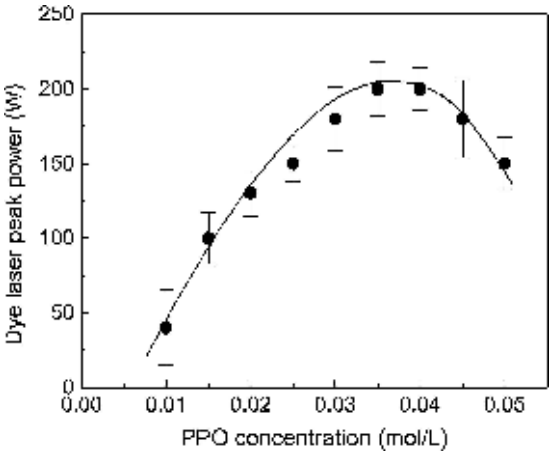

Figure 15 Dye laser peak power of inorganic alumina films doped with both PPO and α-NPO as a function of donor dye (PPO) concentration. Acceptor dye (α-NPO) concentration is 8×10^{-3} mol/L. Each film contains 10 wt% of CTAB. Reprinted from *Nippon Kagaku Kaishi* (1992) 1257.

PPO concentration in the range above 3.5×10^{-2} M. Probably, all the donor PPO molecules were not excited at high PPO concentration, and then the non-excited PPO molecules brought about a quenching of the excited PPO molecules. This behavior may be described as concentration quenching. Beside the pair of PPO-α-NPO, pairs of R6G-RB and C1-uranine also exhibited energy-transfer-type laser emission.

4.3. Hole-burning

Hole-burning has been attracting a great deal of attention as new spectroscopies provide us with more information on the dynamics of microstructures in amorphous matrices at low temperatures [91, 92]. In

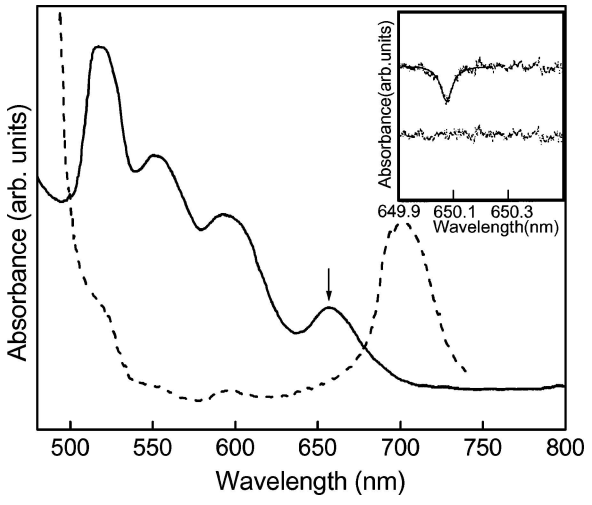

Figure 16 Absorption spectrum of 10^{-2} M TPPS-doped inorganic alumina film. Inset shows a hole profile at 5.0 K. Lorentzian fitting to hole shape is also shown under the hole profile. Flatness of the residual sum of squares indicates good fitting. Reprinted from *J. Non-Cryst. Sol.* **109** (1989) 164.

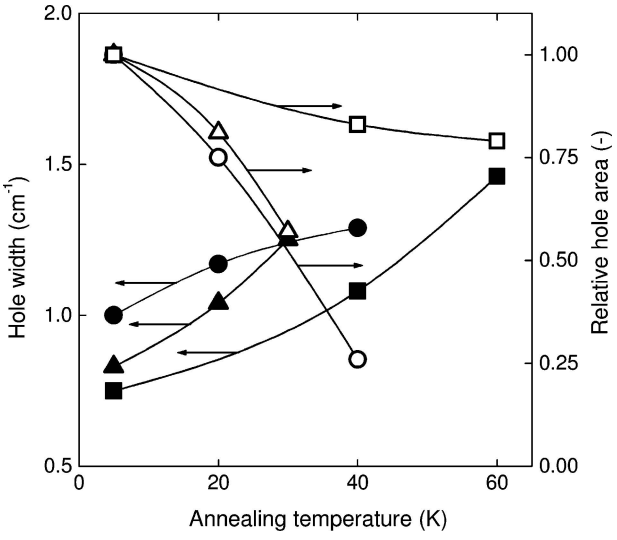

Figure 17 Annealing temperature dependences of changes in hole width and area during the temperature cycle. The hole area at each temperature is normalized with that at 5.0 K. Circles: DNQ, triangles: resorufin, squares: TPPS. Reprinted from *J. Non-Cryst. Sol.* **109** (1989) 164.

addition, application of hole-burning materials for high-density optical data storage has been expected [92]. A candidate for the hole-burning materials is dye-doped films. For host films, various organic and inorganic films have been reported to date [91]. It is known that the rotational and translational freedom in host network is responsible for hole filling and broadening well below liquid N_2 temperature [93–98]. On the other hand, interaction between dye molecules at high concentrations results in hole broadening and in lowering of hole burning efficiency [92]. In the practical use of hole-burning memory, a highly concentrated doping of dye without aggregation is necessary for fast writing of memory, and rigidity in the host network is required for high thermal durability than films such as organic polymers. Development of the sol-gel process using alkoxide (especially tetraethyl silicate) opened a possibility to use an inorganic matrix instead of organic polymers as a hole-burning material. However, the aqueous sol solution route has not yet been well described compared with the alkoxide route. The aqueous solution route is readily available and inexpensive. In this section, we describe application of our inorganic alumina film for a hole-burning host [14].

The absorption spectra of TPPS-doped inorganic alumina are shown Fig. 16 [14]. The original TPPS spectrum (dashed line) corresponded to TPPS with four protonated inner *N* atoms. Such film did not show a hole-burning effect. Because tautomerization has to take place in hole-burning of porphiline by laser irradiation, porphiline should have two protonated inner *N* atoms. Since acetic acid was contained in the alumina sol solution, pH in the alumina film was in acidic range. The spectrum after NH_3 gas treatment had four peaks that corresponded to TPPS with two protonated *N* atoms. Then, a hole was observed for the NH_3 gas treated film as shown in the inset. Besides TPPS, spectra of 5,8-Dihydroxy-1,4-naphthoquinone and resorufin and $\alpha,\beta,\gamma,\delta$-tetrakis (4-sulphophenyl) porphine in the alumina films were also hole-burned, respectively.

A temperature cycle experiment was performed to investigate hole profiles as follows: a hole was burned at 5 K, and then the temperature was elevated quickly to various temperature (T_a). After being kept for 5 min at T_a, the films were recooled quickly to 5 K. The changes in integrated hole area and hole width were evaluated for holes at 5 K after each cycle by using Lorentzian function fitted to the hole profile. A cycle experiment reveals irreversible change which is caused by spectral diffusion and/or by backward reaction of photoproducts [97]. Microstructures in amorphous solids have been frequently modeled by a distribution of asymmetric intermolecular double-well potential (two-level system (TLS) model) [99]. Spectrum diffusion results from redistribution of ground states of TLS [97, 100]. Fig. 17 shows temperature dependences of the hole profiles [14]. Irreversible change was found to be prominent in the first cycle and did not depend on the number of cycles when repeated cycling to the same temperature. Therefore, the irreversible change seemed to be caused mainly by some thermally activated processes. The TPPS had a greater thermal durability than DNQ and resorufin and the latter two had the same durability. It can be considered that potential surfaces of ground state TLS associated with DNQ and resorufin were more remarkably changed when the motions of the oxygen and the hydroxyl groups were thermally activated. Furthermore, these motions probably caused backward reactions for DNQ and resorufin. These processes may have explained why the hole filling and broadening were more prominent in the DNQ and resorufin-doped alumina films.

4.4. Nonlinear optics

There have been many investigations of nonlinear optical (NLO) organic materials [101]. However, it is generally difficult to grow NLO molecules in a macroscopic large crystalline form. Therefore, transparent films doped with NLO materials appear to have promise for

integrated optical and waveguide applications. Techniques to enhance NLO properties have not been yet well established. The most practical method is to apply an electric field to a glassy polymer film doped with NLO molecules [102]. In this method, the doped film is heated around a temperature of glass transition, where the dopants are mobile and susceptible to orientation in an applied electric field. Then, the film is cooled under the electric field to fix the polar alignment. The orientation of dopant allows enhancement of second harmonic generation (SHG). However, the SHG intensity decays with an increase in time, due to relaxation of the matrix [102]. On the other hand, it is reported that interaction of NLO molecules into a host layer leads to an oriented arrangement of the molecules [103]. However, the amount of the intercalated molecules is limited and thereby the NLO properties are not enough. Several approaches have been taken to prepare hybrid gels comprised of organic and inorganic components for optical materials [88, 104]. 2-Methyl-4-nitoaniline (MNA) is incorporated in a SiO_2-polymethyl methacrylate film. The MNA-doped film retains optical quality at higher temperatures and is more resistant to abrasion [105]. In this section, we show NLO properties of various NLO dyes-doped inorganic alumina films.

MNA molecules were dispersed into the inorganic alumina films in the presence of a surface active agent, CTAB, since MNA is insoluble in water [23]. Neodymium-glass laser ($\lambda = 1064$ nm) was used for irradiation. In the alumina films doped with dopants such as laser dye and hole-burning dye, the dopants were usually dispersed at a molecular level. However, the MNA molecules were finely microcrystalized in the alumina, since the MNA-doped film exhibited a weak SHG effect. To orient the MNA microcrystallites in the film, an electric field of 8 $kVcm^{-1}$ was applied to the film at 110°C by the corona poling method, and the temperature was decreased down to room temperature under the application of the electric field, so that the orientation of MNA was retained. Its SHG intensity was one order of magnitude higher than that of the non-poled film. The SHG transformation efficiency from the fundamental laser to the second harmonic generated laser was around 2×10^{-7}%. Crystalinity of MNA molecules is improved and its SHG effect is enhanced by co-doping MNA and a few % of *p*-nitroaniline (*p*-NA) [106]. For the inorganic alumina, co-doping MNA and *p*-NA at 10 mol% for MNA was performed. Its SHG intensity was about 20 times higher than that of the poled MNA-doped film. The crystallite of *p*-NA itself does not exhibit SHG effect, since the crystallite has an inversion center. In addition, the co-doped film was not treated with the corona poling method. Dipole moment of each MNA molecule was probably aligned to produce overall moments that direct the polar axis as a result of interaction between MNA microcrystallites and *p*-NA molecules. This alignment seemed to cause the enhancement of SHG.

N-(4-nitrophenyl)-*L*-prolinol (NPP) was also used as a NLO dopant [27, 28]. NPP is a *p*-nitroaniline-like substance which has a π-electronic aromatic system involving donor (prolinol) and acceptor (nitro) substituent groups, and its properties relate to those of MNA analogs [107]. Fig. 18 shows XRD pattern of NPP-doped inorganic alumina films. The doped film without annealing showed no XRD peaks, which indicated that NPP molecules were finely distributed in the CTAB micelle. By annealing the film at 100°C, which was lower than the melting point of NPP (116–117°C), and then cooling down to room temperature, the NPP crystallites grew by an Ostwald ripening effect and gave XRD peaks. The film shrank by thermal dehydration and the micelles were probably distorted, which seemed to induce the NPP molecules to be crystallized. The NPP microcrystallites in the film exhibited a preferred crystalline (101) orientation of an orthorhombic structure. The highest peak was obtained at 3.5 wt% NPP and 8.75 wt% CTAB. Since NPP tends to take a plate-like crystalline form, the NPP molecules were expected to be stacked lying parallel to the alumina layers. At an annealing temperature of 130°C, the highest XRD peak of NPP was observed at 2.5 wt% NPP and 6.25 wt% CTAB, that were lower than the 100°C-annealed film. The high annealing temperature probably accelerated the crystallite growth of NPP. NPP crystallization and crystalline growth took place even at lower concentrations than the case of 100°C. However, the NPP microcrystallites might have been incorporated more finely into the microstructure of the film, since the microcryatallites must be melted at 130°C. As a result, a number of crystallites smaller than the case of 100°C were formed during cooling down. Therefore, the concentration that provided the highest (101) peak intensity shifted to lower concentration compared with 100°C-annealing. Fig. 19a show a typical SHG Maker fringe

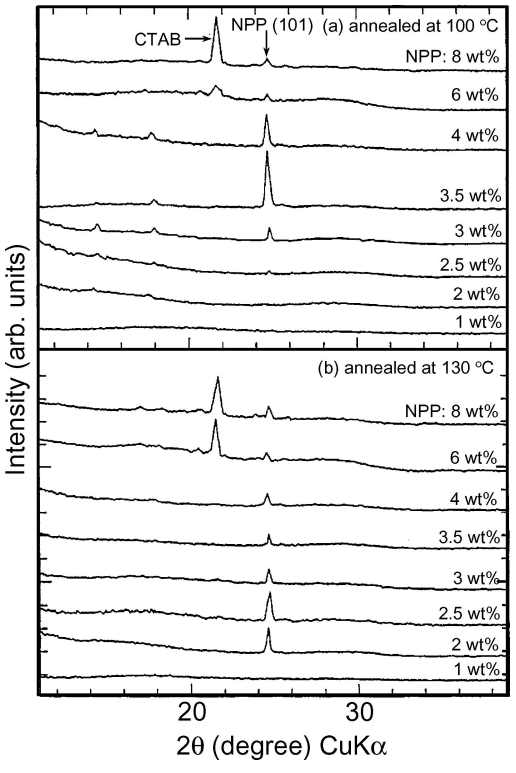

Figure 18 XRD patterns of NPP-doped inorganic alumina films at definite ratio of CTAB/NPP = 1:2.5. Annealing time was 2 h. Reprinted from *Thin Solid Films* **283** (1996) 221.

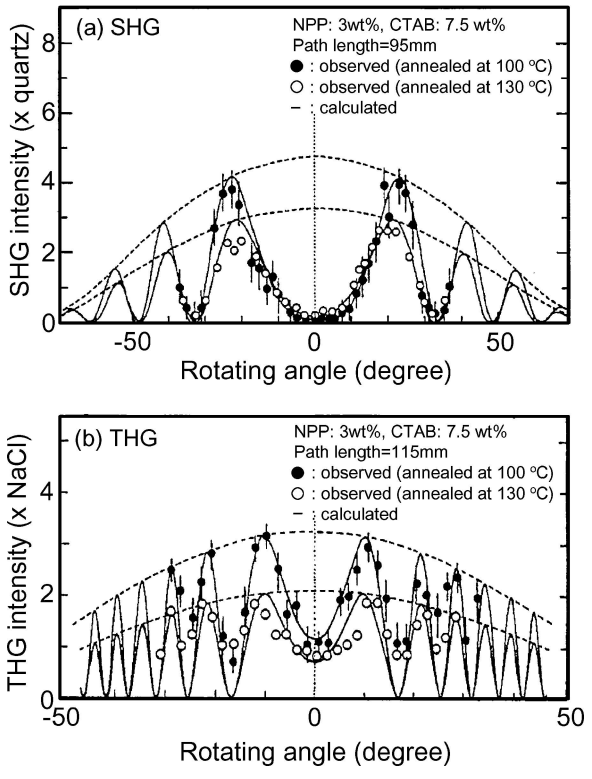

Figure 19 Typical SHG (a) and THG (b) Maker fringe patterns of NPP-doped inorganic alumina films. Reprinted from *Thin Solid Films* **283** (1996) 221.

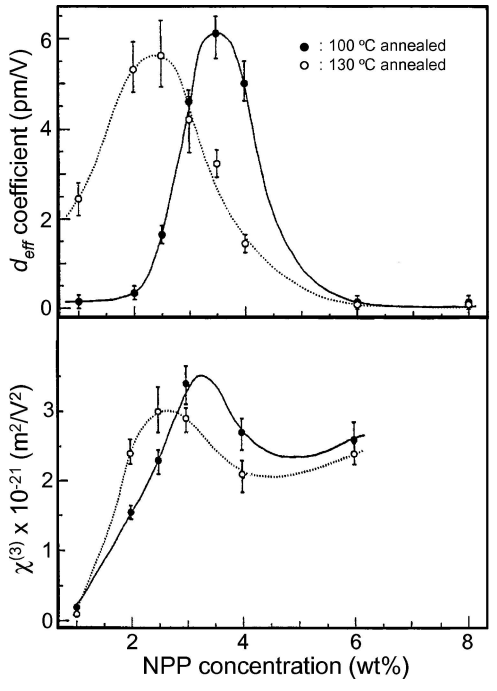

Figure 20 Second order NLO coefficient d_{eff} (a) and third order NLO susceptibility $\chi^{(3)}$ (b) of NPP-doped inorganic alumina films. Reprinted from *Thin Solid Films* **283** (1996) 221.

pattern of NPP-doped alumina films. The patterns were in good agreement with the calculation from the theoretical expression of Jerphagov and Kurtz [108, 109]. Second order NLO coefficient, d_{eff}, was estimated by comparing the signal intensity of quartz. Fig. 20a shows d_{eff} as a function of NPP concentration. Maximum d_{eff} was 6.1 pmV^{-1} (1.5×10^{-8} esu) for the 3 wt% NPP-doped alumina annealed at 100°C. In both cases, the concentration that gave the highest d_{eff}, corresponded to the concentration with the highest XRD intensity of NPP (101) phase. This recalls that crystallite orientation of NLO molecules, which leads to increasing of sum of dipole moments of each molecule, is absolutely necessary to enhance SHG effects.

An interest has been arisen in third-order NLO materials such as semiconductor particles-doped glass, polysilane or polydiacetylene [101]. In the case of macromolecules, third-order nonlinear susceptibility, $\chi^{(3)}$, increases with an increase in the length of the π-electron conjugated chain. Investigations of low-molecular weight NLO materials have been rarely found in the literature because they have lower susceptibities compared to the NLO macromolecules. Third-order NLO properties can be observed even in optically isotropic materials in which the dipole moment is cancelled out, and it has been thought that third-order properties are independent of molecular orientation. However, $\chi^{(3)}$ depends on the conformation within the overall structure in the case of polydiacetylene [110]. In this section, we introduce our investigation of third-order NLO properties of the NPP-doped alumina film.

Fig. 19b shows typical fringe patters of THG intensity. $\chi^{(3)}$ was estimated by comparing the signal intensity of NaCl crystal. Fig. 20b shows $\chi^{(3)}$ as a function of NPP concentration. Maximum $\chi^{(3)}$ was 3.3 m^2V^{-2} (2.5×10^{-13} esu) for the 3 wt% NPP-doped alumina annealed at 100°C. In both films annealed at 100°C or 130°C, the concentration that gave the highest $\chi^{(3)}$ corresponded to the concentration with the highest XRD intensity of NPP (101) phase, as well as d_{eff}. In other words, the higher degree of NPP molecule oriented, the more intense THG. That analogy between the behavior of SHG and THG for the doped film may be explained by the cascade process of SHG. In the range of the ordered NPP-doped film, an enhancement of THG was possibly not due to a direct THG process ($\omega + \omega + \omega - 3\omega$) from the source light (ω), but to a cascade combination of twoSHG processes ($\omega + \omega - 2\omega$, $2\omega + \omega - 3\omega$). These results indicated that the molecular alignment contributed not only to SHG but to THG, and illustrated the importance of crystal design in third-order NLO materials, as well as second-order NLO materials.

Besides MNA and NPP, Disperse Red 1 (DR1) was used as a dopant for third order NLO materials [32]. The DR1-doped inorganic alumina film was examined by the degenerated four-wave mixing method using the second harmonics (532 nm) of a Nd-YAG laser. The DR1-doped film showed an absorption peak that was close to 532 nm. Therefore, its third-order nonlinear property at 532 nm was enhanced by resonance effect, and gave a high $\chi^{(3)}$ value of around 10^{-7} esu.

5. Nanoparticles-doped alumina films

5.1. Introduction

Colloidal nanoparticles have special interest in science and technology because they exhibit unique optical and

catalytic properties that are different from those of the bulk materials [111–117]. Properties of these nano particles can be preserved if the general tendency for aggregation can be overcome, such as if a suitable stabilization can be developed. Generally, the stabilization of colloids is performed by surface modification processes, either to enhance double-layer interactions or to adsorb macromolecules that can form a physical barrier against other approaching particles [118]. A method for obtaining colloidal stabilization is loading nanoparticles in a solid state matrix. The role of the solid state matrix prevents the particles from aggregating through a physical barrier of the solid matrix. From this point of view, extensive studies on a solid state film loaded with nanoparticles have been made. In this section, we introduce preparations of alumina films doped with various nanoparticles with a sol-gel process and their several properties such as catalysis and optics [10, 11, 17, 21, 25, 26, 29, 30, 32, 39].

5.2. Catalysis

There have been some investigations of highly dispersed metal catalysts [119–121]. Investigations of highly dispersed metal catalysts supported on silica prepared using tetraethyl silicate are limited exclusively to the catalysts for gas reactions [121]. Besides silica, the gel prepared from nickel acetate and aluminum sec-butoxide is quite dense and was not very active for the hydrogenation of nitrobenzene [119]. However, the aqueous alumina sol using inorganic salts has not been used as a starting material of alumina support as well described as the alkoxide route. The inorganic alumina sol are readily available and inexpensive, it is worth being used as a precursor of the solid state matrix. In this section, we introduce preparation of a new type of catalyst consisting of the inorganic alumina dispersing fine nickel particles uniformly [10, 11].

The inorganic alumina sol mixed with $Ni(NO_3)_2$ was converted to gel by slow evaporation of water. The gel was annealed in a stream of hydrogen for 2 h at 400°C. The annealing resulted in a black powder. Since XRD peaks of metallic nickel were detected, the color change was due to reduction of nickel ions to metallic nickel. Fig. 21 shows TEM image of the Ni-doped alumina. Nickel nanoparticles with sizes of 5–25 nm were observed. According to XPS analysis, the Ni loading was 30 wt% at highest. This new catalyst showed higher selectivity in the liquid phase hydrogenation of 1,3 and 1,5-cyclooctadiene and methyl linolenate than either Raney nickel or impregnated nickel-alumina catalysts. However, it showed lower activity than Raney nickel. This phenomenon may be attributed to the coating of nickel particles with alumina matrix.

5.3. Optics

It has been suggested that the third order NLO of semiconductor particles is enhanced when a three dimensional confinement of electron-hole is fulfilled in the semiconductor particles [122–124]. Development of this investigation is important in a view of applications such as switching devices in optical waveguides and the phase conjugator medium in optical computer devices.

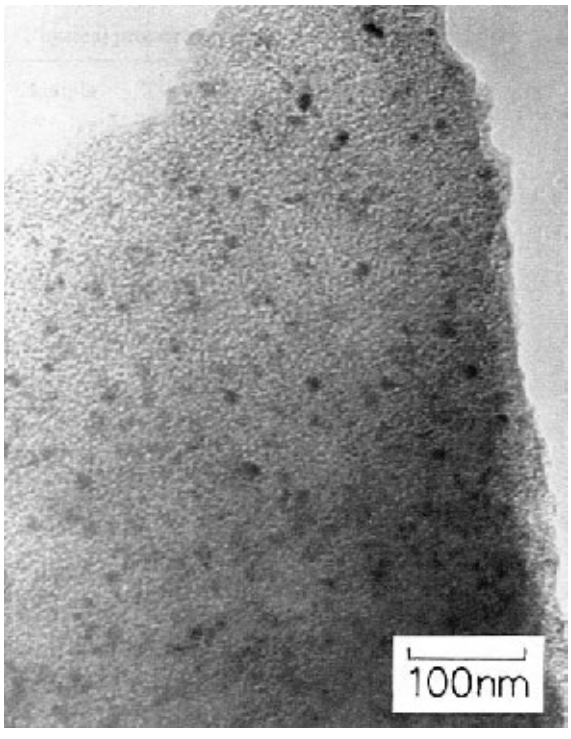

Figure 21 TEM image of Ni-loaded inorganic alumina obtained from the thermal decomposition at 450°C in hydrogen stream (Ni content: 10 wt%). Reprinted from *Appl. Catal.* **40** (1988) 139.

Semiconductor nanoparticles, i.e., CdS nanoparticles, which are one of semiconductor intensively studied, were synthesized in an alumina film as follows [17, 21]. The inorganic alumina sol was mixed with $Cd(CH_3COO)_2 \cdot 2H_2O$ or $Cd(OH)_2$ to yield 1–10 wt% for the films. After gelation in air at 40°C, the gel film was annealed in a stream of H_2S gas at a temperature of 100–600°C, which led to formation of a yellowish film (Fig. 12). According to XRD patterns, the color change to yellow was due to production of CdS particles and their crystalline sizes were estimated around 6.5 nm for 300°C-annealed CdS-loaded alumina and 8.0 nm for 400°C-annealed. The particle sizes observed in TEM were in the range of 6–10 nm, in agreement with the crystalline sizes. Wavelength shift of the absorption edge by a quantum size effect was clearly observed in the absorption spectra in visible wavelength range. The largest refractive index change of -1.3×10^{-3} was obtained at a band edge of the absorption spectrum (300°C-annealed) with 1.46 $MWcm^{-2}$ pumping because of a band filling effect. Through the investigation by degenerate four-wave mixing (DFWM) technique, the observed spectrum of the DFWM diffraction efficiencies agreed well with the values calculated from the measured absorbance change and reflectance index change at a small absorption region.

The noble metallic nanoparticles give rise not only to the color change but also to optical enhancements in absorption, Raman scattering, and luminescence effects. Much attention has been paid to the study on optical properties of nanoparticles dispersed in glass and polymer matrices from the viewpoint of scientific interest and their applications to nonlinear optical devices [125–128]. Most of works on glass are concerned exclusively with silicate glass. However, experiments for NLO properties of metal particles-loaded alumina film have been rarely found in publications. Coinage metal nanoparticles such as Au or Ag were doped in an alumina film as follows [29, 32]. Aqueous $AgNO_3$ or $HAuCl_4$ solution was mixed with the transparent inorganic alumina sol. The mixture was poured on a flat plate such as a polystyrene petri dish. It was then converted into an alumina gel film doped with $AgNO_3$ or $HAuCl_4$ by dehydration in an atmosphere at room temperature. These $AgNO_3$ or $HAuCl_4$-doped alumina film was then annealed in H_2 gas in a reaction silica tube under raising temperature from room temperature to desired temperatures of 300–800°C. After reached to the desired temperature, the temperature was kept constant for 2 h. Fig. 22 shows TEM image of Au particles-doped alumina film. Observed particles were approximately spherical in shape. The average particle sizes were in the range of 4.6–12.8 nm and increased with an increase in the annealing temperature. XRD measurements revealed a peak that was attributed to the (111) plane of cubic Au structure, which indicated that the spherical particles were metallic Au. The particle sizes agreed well with crystal sizes that were determined from Scherrer's equation for the XRD results. Similar observations of TEM and XRD were also made for the Ag-doped alumina. The Ag- or Au-contained alumina films showed color change that depended on the annealing temperature. These colors were attributed to surface plasmon absorption of noble metal nanoparticles. The surface plasmon absorption band is very sensitive both to particle size and shape and to properties of the surrounding medium [129–133]. Plasmon band of noble metal nanoparticles dispersed in a dielectric medium is expressed by a Mie-Drude equation [130]. Peak broadening and peak shift of the plasmon spectra for the Ag-doped alumina films were in agreement with the Mie-Drude equation [39]. Fig. 23 (A) shows absorption spectra of the Au-doped films [29, 32]. Peaks in the range of 520–650 nm were due to the surface plasmon band. The spectra broadened and the peak shifted to longer wavelength (red shift) with a decrease in the particle size. This behavior was opposite to that observed in the case of Au particle-doped silicate glass [130, 134]. This shift was toward the opposite direction from predicted by the Mie-Drude model. The classical Mie theory, using the Drude expression for the dielectric function of particle, can be well applied to the particle dispersed system [134]. In the Mie equation the absorption cross section is

$$\sigma_{\mathrm{abs}}(\omega) = 9k\varepsilon_0^{3/2} V_0 \frac{\varepsilon_{\mathrm{m2}}(\omega)}{[\varepsilon_{\mathrm{m1}}(\omega) + 2\varepsilon_0(\omega)]^2 + \varepsilon_{\mathrm{m2}}(\omega)^2}, \tag{3}$$

where k and V_0 are the wave vector and particle volume, ε_0 and ε_{m} $(= \varepsilon_{\mathrm{m1}} + i\varepsilon_{\mathrm{m2}})$ are the dielectric functions of the matrix and metal particle, respectively. The Drude expression is

$$\varepsilon_{\mathrm{m,free}} = 1 - \frac{\omega_{\mathrm{p}}^2}{\omega^2 - i(\omega/\tau)}, \tag{4}$$

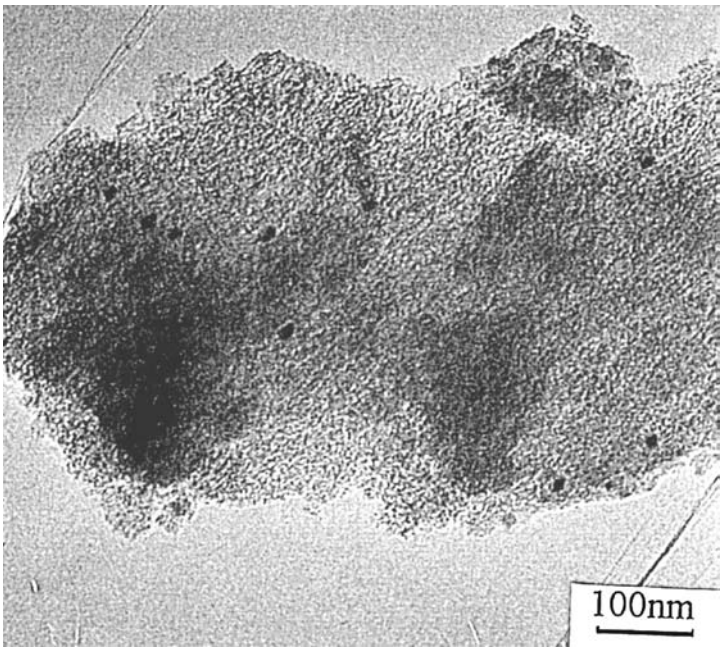

Figure 22 TEM image of Au particles-doped inorganic alumina film. The Au concentration is 0.4 mol% for alumina. The film was annealed at 600°C in air. Reprinted from *Thin Solid Films* **322** (1998) 233.

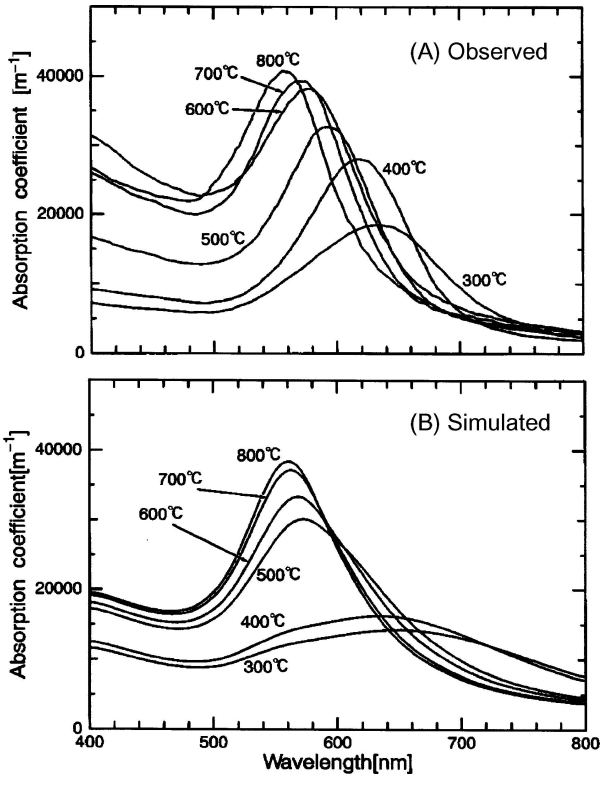

Figure 23 Plasmon spectra of Au particles-doped alumina films. Au concentration is 0.1 mol% for alumina. (A) Observed and (B) simulated by using the two region model. Reprinted from *J. Appl. Phys.* **81** (1997) 1475.

where τ is a relaxation time and ω_p is the plasma frequency. It assumes that the metal contains free electrons that move restrictively by the positive lattice. The Mie-Drude prediction taking into account the dielectric constants of the bulk metal and of the matrix can be applied to explain the plasmon absorption peak. A common way to fit experimental data with the Mie equation is by introduction of a size-dependent electron relaxation time in terms of the scattering at the surface; however, it cannot explain the large blue shift or size dependence of peak width evident in Fig. 23 (A). The Mie-Drude expression yields the following plasmon frequency [130, 135]:

$$\omega_M = \frac{\omega_p}{\sqrt{\varepsilon_b + 2\varepsilon_0}}, \tag{5}$$

where ε_b is the dielectric constant of bound electron. The electric constant of alumina ε_0 would not change significantly by annealing at 300–800°C. The ω_p is given as

$$\omega_p = \left(\frac{4\pi n_e e^2}{m_e}\right)^{1/2}, \tag{6}$$

where n_e and m_e are the density and mass of electron, respectively. The ω_p and n_e are obtained from fitting with the observed spectra. Considering a relation between n_e and particle size, the electron density decreases with a decrease in the particle size. The density profile is not modeled only by the particle size, form, or dielectric constants, but by the details of the surface surrounding particle. That is, physisorption, chemisorption, or another chemical interface interaction may induce the change of the electron density profile. Surface interactions including charge transfer to or from the particle, which change the peak width strongly [130], would be remarkable in an aqueous sol. In metal-alumina ceramic adhesion, two main bonds of O–M and Al–M are responsible for the adhesion strength of the interface [136]. The former interaction is repulsive, while the latter is attractive. To stabilize the adhesion energy, the electron transfers into a dangling bond on Al. In the inorganic alumina that was in amorphous state, many dangling bonds probably existed in matrix. On the other hand, the direction of shift (red or blue) are explained by taking into account the spill-out or -in of the free electron through the particle surface, affected by the matrix [135, 137–139]. This gives the microscopic description for the two-region (core-shell) model in which the particle is approximated as containing an inner core region characterized by bulk like core dielectric functions and an outer shell region where the core polarization is ineffective [137]. When the free electron transfers from the particle to the matrix, the density of the free electron is reduced and then the dielectric function of the free electron can be regarded as having been missed in an outer region near the particle surface. It reduces the electron density and thereby the resonance frequency. Equation 3 is modified to Equation 7 based on a two-region model, similar to the case of Ag particles embedded in a rare gas matrix [137],

$$\sigma = 9ke_0^{1/2}V_0 \,\mathrm{Im}\left(\frac{(e_{m,free} - e_0)(e_m + 2e_{m,free}) + f(e_m - e_{m,free})(e_0 + 2e_{m,free})}{(e_{m,free} + 2e_0)(e_m + 2e_{m,free}) - f(e_m - e_{m,free})(2e_0 - 2e_{m,free})}\right), \quad f = \left(\frac{r}{r+a}\right) \tag{7}$$

where a is the thickness of outer region. The outer region is a sort of mixing layer of particle surface with dangling bond of alumina. This layer corresponds to an adhesion boundary layer in adhesion of ceramic with metal.

The peak broadening is due to the spatial spreading and scattering of the electron across the particle-matrix interface [136]. The range of scattering (which is a measure of polarizability) is treated by adding or subtracting a spill-out distance to the particle size. In this theory, the free electron which contributes to plasmon absorption and is spilled out into the matrix is relaxated in its energy by the surrounding matrix before being scattered and returned into core particle.

In the calculation of the absorption spectra using Equation 7, the peak shift depended on the thickness of the outer region; thick outer region brought about large blue shift. We took a mean value as a representative

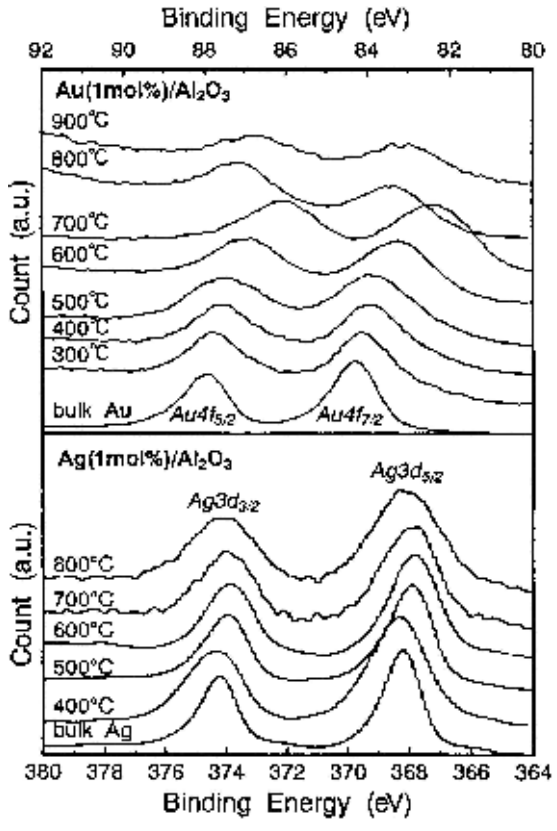

Figure 24 XPS spectra (Au4f) of Au particles-doped alumina films and those (Ag3d) of Ag particles-doped alumina films annealed at various temperatures. Reprinted from *Opt. Communic.* **190** (2001) 385.

diameter for calculation. The calculated spectra using $a = -0.5$ nm for the thickness of the outer region are shown in Fig. 23 (B), which was in fair agreement with Fig. 25 (A).

Fig. 24 shows XPS spectra of Au4f for Au-doped alumina and those of Ag3d for Ag-doped alumina films [39]. With an increase in annealing temperature, the Au4f peaks underwent a significant shift to the lower energy side and then a significant shift to higher energy side. The shift was the largest at the temperature at which γ-alumina was formed. This result indicated that the electron density in Au particles increased with an increase in annealing temperature, and supported the explanation for the peak shifts of plasmon. However, the Ag3d peak did not shift significantly. There are some publications suggesting a strong interaction between Au and Al [140–142]. The noticed Au4f peak shift in the Au-doped inorganic alumina was probably due to such strong interaction.

The Au particles-contained inorganic alumina films were examined by the DFWM method [29, 30, 39]. Fig. 25 shows the third-order susceptibility $\chi^{(3)}$ values estimated at various wavelengths (530, 550 and 570 nm). A resonance enhancement was observed in the vicinity of the surface plasmon band. The electric field inside the particle, E_1, is explained with the applied field E_0 by

$$E_1 = \frac{3\varepsilon_0}{\varepsilon_m + 2\varepsilon_0} E_0. \quad (8)$$

Thus, E_1 is enhanced near the surface plasmon resonance of the Au particle. This enhancement of the

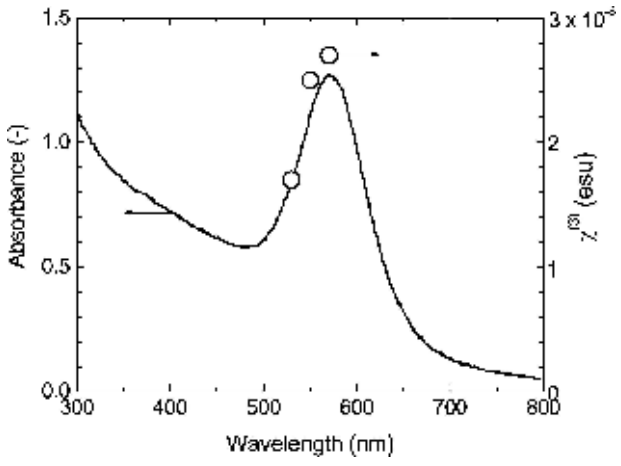

Figure 25 $\chi^{(3)}$ values at near plasmon spectra of Au particles-doped alumina film annealed at 700°C. The Au concentration is 0.1 mol% for alumina. Reprinted from *J. Appl. Phys.* **81** (1997) 1475.

electric field inside the particle probably led to the resonance enhancement.

The inorganic alumina films doped with Au particles of various sizes were characterized with the DFWM method [29]. However, there was no clear size-dependence observed. Three mechanism have been proposed as major contributions to $\chi^{(3)}$: hot electron, interband and intraband transitions [143, 144]. The first two effects have been shown to be nearly size-dependent. Only the intraband transition can explain the size-dependence of $\chi^{(3)}$. The experimental evidence indicated that the conjugate reflectivity of Au colloid was independent of particle size and that the important parameter was the colloid concentration. It should be necessary to take into account the effect including the Au particle-alumina interface.

Table I shows $\chi^{(3)}$ values of Ag or Au-doped alumina films. The values $\chi^{(3)}$ and $\chi^{(3)}/\alpha$ (α: absorption coefficient) were on the order of 10^{-8} esu and 10^{-10} esu · cm, respectively. Both values for the Au-doped alumina were larger than for the Ag-doped alumina. This was mainly due to the enhanced local field near the Au plasmon band. The value for the Au particle should be one order larger than that for the Ag particle according to the literature. However, the $\chi^{(3)}$ and $\chi^{(3)}/\alpha$ for the Au-doped alumina were not so large compared to those for the Ag [143], which might have been partially to a decrease in electron density by electron transfer to the alumina surface.

TABLE I The third-order susceptibilities of noble metal particle-doped alumina films. Reprinted from *Opt. Communic.* **190** (2001) 385

Metal (treat-temperature)	Metal content (mol%)	$\chi^{(3)}$ (esu)	$\chi^{(3)}/\alpha$ (esu · cm)
Ag (700°C)	0.3	2.5×10^{-8}	1.9×10^{-10}
	0.4	5.3×10^{-8}	2.6×10^{-10}
	0.5	1.9×10^{-8}	0.95×10^{-10}
Au (800°C)	0.1	3.5×10^{-8}	4.1×10^{-10}
	0.2	9.0×10^{-8}	7.1×10^{-10}
AU (400°C)	0.2	3.2×10^{-8}	2.0×10^{-10}

α: absorption coefficient.

6. Rare earth ion-doped alumina films

6.1. Introduction

Optical properties of rare earth (RE) ion-doped silica glasses have been studied extensively for use in lasers and optical devices [144–147]. The sol-gel method can fabricate silica glass with higher dopant concentrations than conventional melt glass. Clusters of the dopant ions are formed both in sol-gel and conventional glasses at higher concentrations. The clusters provide shorter decay time and quenching of luminescence. Co-doping with alumina for the glass was found to enhance the dispersion of rare earth ions and thereby luminescence properties were improved [148–151]. In addition, alumina has a high transparency from UV to near IR wavelength and higher thermal conductivity compared to SiO_2 glass. Therefore, alumina is expected to be a good matrix for rare earth ions. In this section, we introduce fabrication of rare earth ion-doped alumina films and their luminescence properties [34–40].

6.2. Luminescence properties under various conditions

Luminescence efficiencies for RE ions-doped glasses depend on matrices, e.g., phonon energy, amount of hydroxy groups, dispersity of RE ions and symmetry of crystal field around RE ions. These properties are varied by preparation conditions, i.e., annealing temperatures and doped rare earth concentrations. Alumina films were doped with various RE ions such as Pr^{3+}, Nd^{3+}, Sm^{3+}, Eu^{3+}, Gd^{3+}, Tb^{3+}, Dy^{3+}, Ho^{3+}, Er^{3+} and Tm^{3+} and their luminescence properties were investigated. Fig. 26 shows luminescence spectra for Eu^{3+}-doped alumina films annealed at various temperatures and various Eu^{3+} concentrations. Luminescence spectra had peaks assigned to ${}^5D_0 \rightarrow {}^7F_0$ (577 nm), ${}^5D_0 \rightarrow {}^7F_1$ (588 nm), ${}^5D_0 \rightarrow {}^7F_2$ (614 nm), ${}^5D_0 \rightarrow {}^7F_3$ (651 nm) and ${}^5D_0 \rightarrow {}^7F_4$ (699 nm) transition. These peaks were broader than luminescence peaks observed in crystalline matrices, reflecting the amorphous property of the sol-gel alumina films. Luminescence intensities based on these transitions increased with an increase in the annealing temperature and the concentration. The annealing probably led to liberation of free and coordinated water and to crosslinking between alumina by the removal of residual OH groups on alumina (dehydroxylation). With high loading of the RE ions, the RE ions became partially substitute-coordinated with the OH groups of the alumina. It can be considered that the amount of OH groups that brought about large phonon relaxation was reduced in the films and thereby the luminescence intensities at high annealing temperature and large concentration. The ${}^5D_0 \rightarrow {}^7F_2$ and the ${}^5D_0 \rightarrow {}^7F_1$ transitions are an electric dipole transition and a magnetic dipole transition, respectively. Because these transitions are sensitive and insensitive to symmetry of the ligand field around Eu^{3+}, the ${}^5D_0 \rightarrow {}^7F_2/{}^5D_0 \rightarrow {}^7F_1$ luminescence ratio can be used as a measure of the site symmetry of Eu^{3+}. In our system, the luminescence ratio on Eu^{3+}-doped alumina films was dependent on the annealing temperature, but not on concentration. Shrinkage by the removal of OH groups with the heat treatment probably caused distortion of the local environment, viz. an asymmetric character with strong inhomogeneities from site to site. For further investigation, parameters in Judd-Ofelt theory were estimated. A parameter, Ω_2, is dependent on asymmetric structure and parameters, Ω_4 and Ω_6, are dependent on covalency of RE–O bond. A change of Ω_2 corresponded to the changes of the luminescence ratio and the luminescence lifetime. This indicated that RE ions were preferably portioned by Al^{3+}, to form Al–O–RE bonds, rather than RE–O–RE, which supported the distortion of the local environment with the annealing. Effects of the annealing temperature on the luminescence properties was similar for all rare earth ions and similar results on the concentration dependence were obtained for Pr^{3+}, Nd^{3+}, Eu^{3+}, Gd^{3+}, Tb^{3+}, Ho^{3+} and Er^{3+}. However, for alumina films doped with Sm^{3+}, Dy^{3+} (Fig. 27) and Tm^{3+}, luminescence intensities and lifetimes decreased with an increase in their concentrations in the range above 1 mol%. It was confirmed by a quantitative treatment of measured lifetimes that this concentration quenching took place through cross-relaxation. An excited ion (the donor) relaxes nonradiatively to the lower arbitrary level, whereas another ion in the ground state (acceptor) is excited to the higher arbitrary level. These two ions probably cross-relaxed so that energy was conserved by both ions for a while and finally converted into heat, though it is not clear at the moment why

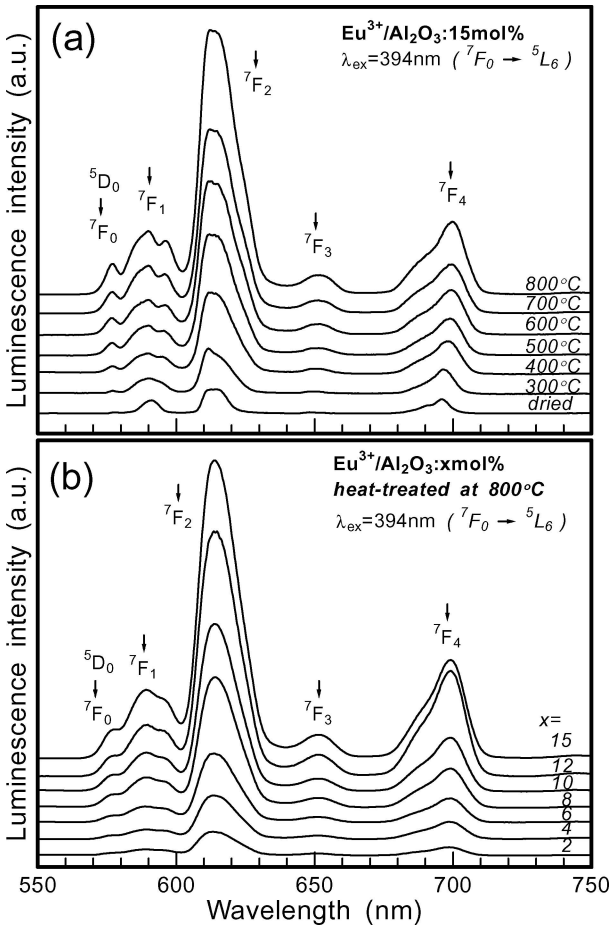

Figure 26 Luminescence spectra for Eu^{3+}-doped inorganic alumina films annealed at various temperatures (a) and various Eu^{3+} concentrations (b). Reprinted from *J. Appl. Phys.* **90** (2001) 243 and *Hyomen* **39** (2001) 326.

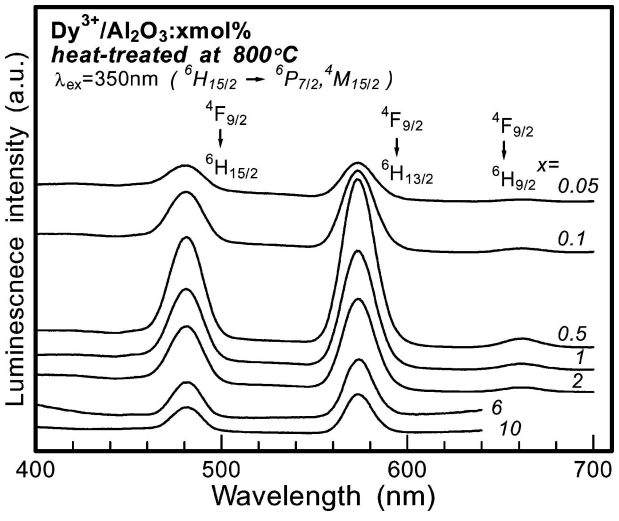

Figure 27 Luminescence spectra of Dy^{3+}-doped inorganic alumina films under various Dy^{3+} concentrations. Reprinted from *J. Luminesc.* **92** (2001) 57.

these RE ions-doped alumina films showed significant cross-relaxation.

6.3. Upconversion luminescence

Upconversion luminescence from rare earth ion-doped matrix has attracted considerable attention. Study of the emission process is important for understanding the transition state and the interaction of ions with matrix. Among matrices available to date, fluoride glasses have been extensively investigated, since they have low phonon energy and high transparency. However, it is not easy to handle and form the fluoride matrices. A few works on upconversion luminescences have been reported for sol-gel derived SiO_2 glass. In this section, upconversion emission for RE ions-doped alumina films were studied. Fig. 28 shows luminescence spectra for Nd^{3+}(15 mol%) and Er^{3+}(10 mol%)-doped alumina treated at 800°C films under Ti-sapphire laser excitation (800 nm). Luminescence peaks with wavelengths that were shorter than excitation were observed at 550 (Er^{3+}-doped alumina), 640 (Er^{3+}-doped alumina) and 645 nm (Nd^{3+}-doped alumina). It can be concluded by collating their wavelengths with energy levels that nonradiation and upconversion processes on the pumped ions brought about luminescence at the shorter wavelength. These luminescences were observable even at room temperature, since probably RE ions were load in alumina matrices at high concentration and then the phonon relaxation was reduced, as mentioned in the Section 6.1.

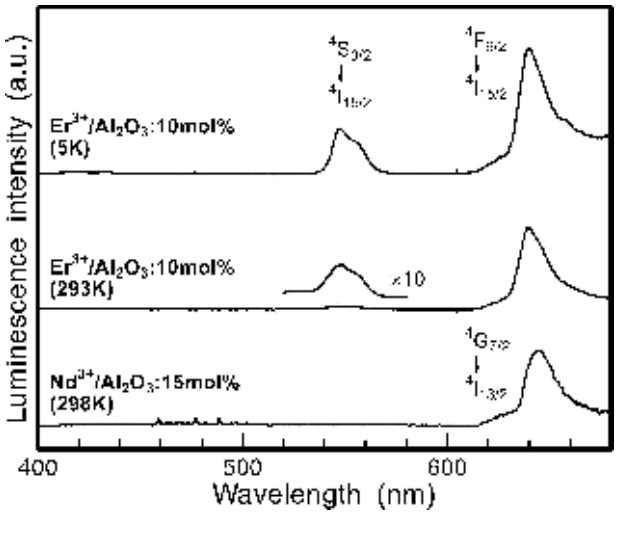

Figure 28 Luminescence spectra for Nd^{3+} (15 mol%) and Er^{3+} (10 mol%)-doped inorganic alumina films annealed at 800°C under Ti-sapphire laser excitation (800 nm). Reprinted from *Opt. Mater.* **15** (2001) 293.

6.4. Sensitized luminescence

For a good efficient energy transfer from exited donor to acceptor, luminescence spectrum of the donor must overlap an absorption band of the acceptor, as mentioned in the Section 4.1. Luminescence peaks of RE ions are so sharp in crystalline matrices that it is hard to make luminescence of RE ions overlap absorbance of another kind of RE ions, compared to organic dyes. Because of broader luminescence peaks of RE ions in the alumina films, well overlapping of a luminescence spectrum of donor RE ions and an absorption spectrum of acceptor RE ions may be possible. Dy^{3+} in our alumina gave concentration quenching due to cross-relaxation beyond 1 mol%. On the other hand, Gd^{3+} increased in luminescence intensity with an increase in its concentration up to 15 mol%. Therefore, we tried to enhance the luminescences of Dy^{3+} by codoping Gd^{3+} into the doped alumina through energy transfer. Fig. 29 shows luminescence spectra for Gd^{3+}-Dy^{3+}-codoped alumina films. Dy^{3+} concentration was constant and Gd^{3+} concentration was varied. Luminescence intensity of Gd^{3+} at 312 nm ($^6P_{7/2} \rightarrow {}^8S_{7/2}$) increased with the Gd^{3+} concentration and decreased above a Gd^{3+} concentration of 9 mol%. In contrary, luminescence intensities of Dy^{3+} at 480 ($^4P_{9/2} \rightarrow {}^6H_{15/2}$), 580 ($^4P_{9/2} \rightarrow {}^6H_{13/2}$), 660 ($^4P_{9/2} \rightarrow {}^6H_{11/2}$) and 770 nm ($^4P_{9/2} \rightarrow {}^6H_{7/2}$) increased with the Gd^{3+} concentration in the whole range of Gd^{3+} concentration examined. It

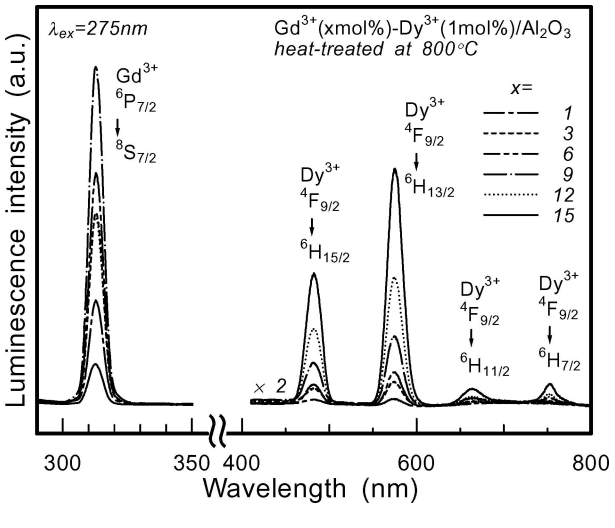

Figure 29 Luminescence spectra for Gd^{3+}-Dy^{3+}-codoped alumina films at various Gd^{3+} concentrations.

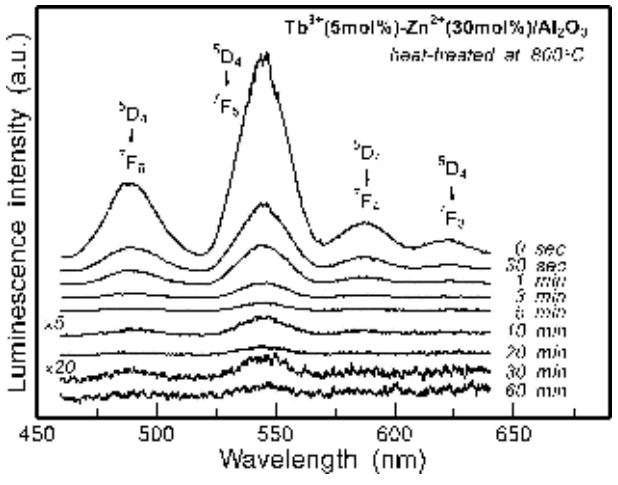

Figure 30 Time dependence of for Tb^{3+} (5 mol%)-Zn^{2+} (30 mol%) alumina film annealed at 800°C. Reprinted from *J. Appl. Phys.* **90** (2001) 2257.

can be considered that this sensitization of luminescence was due to the energy transfer effect, since luminescence bands of Gd^{3+} overlap absorption bands of Dy^{3+} well. Besides, and energy transfer processes from Tb^{3+} to Eu^{3+} and from Gd^{3+} to Sm^{3+} were observed [40].

6.5. Long lasting luminescence

It has been reported that Eu^{2+}-doped alumina silicate and Tb^{3+}-doped alumina silicate glasses prepared in a strong reducing atmosphere gave bright long lasting luminescence [152–155]. However, there have been no observations for the sol-gel derived alumina matrices. In this section, lasting luminescence of RE ions-doped alumina films is mentioned [36].

Tb^{3+}-doped alumina films exhibited lasting luminescence. Addition of Ca^{2+} or Zn^{2+} made the luminescence lasted long. Fig. 30 shows the change of luminescence with time for Tb^{3+} (5 mol%)-Zn^{2+} (30 mol%) alumina film annealed at 800°C. All the luminescence peaks were clearly ascribed to luminescence bands from TB^{3+} ($^5D_4 \rightarrow {}^7F_i$). Lasting luminescence was not detected when the irradiated Zn^{2+}-Tb^{3+}-doped alumina films were immediately immersed into liquid N_2, and the lasting luminescence was detected again at room temperature after the same film was taken out of liquid N_2. Taking into account this finding, a mechanism of the long lasting luminescence can be explained similarly to the mechanism described by Hosono *et al.* [152, 153], as follows.

During light irradiation

$$Tb^{3+} + \text{UV light} \rightarrow (TB^{3+})^+ + e^*,$$

$$e* + \text{oxygen defect center} \rightarrow F^+\text{-like center}.$$

After irradiation

$$F^+\text{-like center} + \text{phonon} \rightarrow \text{oxygen defect center} + e^*,$$

$$e* + (TB^{3+})^+ \rightarrow TB^{3+} + \text{luminescence}.$$

During light irradiation, electrons and holes are formed in the alumina. The holes are captured by in the vicinity of Al^V sites that are oxygen defect sites. The oxygen defect-electron trap depth is broadly distributed and shallow. Therefore, the electrons can be thermally released at room temperature and long lasting luminescence is realized. According to EPR measurement of Tb^{3+}-Zn^{2+}-doped alumina films, an intense signal assigned to an electron trapped at the Al^V sites was detected after the UV-light irradiation at low temperatures, and this signal disappeared by heating at 80°C. This results supported the above mechanism.

7. Conclusions

In this review, we have focused on preparation of alumina films by sol-gel method, their structure, their formation and their various applications. The alumina films themselves were amorphous and very transparent in the range of visible wavelength, and exhibited gas separation ability, good coating property and possibility of hybridizing with organic polymer. In addition, the alumina film matrices enhanced the catalytic and optical properties of guest materials such as organic dye molecules and nanoparticles, because of interactions between guest materials and alumina matrices.

Acknowledgements

The authors are indebted to the many students and collaborators who have actively contributed to the work described in this article.

References

1. "Sol-Gel Science and Technology," edited by M. A. Aegerter, M. Jafelicci Jr., D. F. Souza and E. D. Zanotto (World Scientific Pub., London, 1989).
2. C. J. BRINKER and G. W. SCHERER, "Sol-Gel Science: The Physics and Chemistry of Sol-Gel Processing" (Academic Press, Boston, 1990).
3. "Sol-Gel Processing and Applications," edited by Y. A. Attia (Plenum Press, New York, 1994).
4. "Sol-Gel Optics: Processing and Applications," edited by L. C. Klein (Kluwer Academic Publishers, Boston, 1994).
5. "Biochemical Aspects of Sol-Gel Science and Technology: A Special Issue of the Journal of Sol-Gel Science and Technology," edited by D. Avnir and S. Braun (Kluwer Academic Publishers, Boston, 1996).
6. A. C. PIERRE, "Introduction to Sol-Gel Processing" (Kluwer Academic Publishers, Boston, 1998).
7. Y. KUROKAWA, T. SHIRAKAWA, S. SAITO and N. YUI, *J. Mater. Sci. Lett.* **5** (1986) 1070.
8. F. SUZUKI, K. ONOZATO, J. YANAGINUMA and Y. KUROKAWA, *Koubunshi Ronbunsyu* **43** (1986) 767.
9. F. SUZUKI, K. ONOZATO and Y. KUROKAWA, *J. Non-Cryst. Solids* **94** (1987) 160.
10. J.-I. ISHIYAMA, T. SHIRAKAWA, Y. KUROKAWA, S. IMAIZUMI and S. SAITO, *Nippon Kagaku Kaishi* (1987) 1964.
11. J.-I. ISHIYAMA, Y. KUROKAWA, T. NAKAYAMA and S. IMAIZUMI, *Appl. Cat.* **40** (1988) 139.
12. Y. KOBAYASHI, Y. KUROKAWA, Y. IMAI and S. MUTO, *J. Non-Cryst. Solids* **105** (1988) 198.
13. Y. KOBAYASHI, Y. IMAI and Y. KUROKAWA, *J. Mater. Sci. Lett.* **7** (1988) 1148.
14. H. TANAKA, J. TAKAHASHI, J. TSUCHIYA, Y. KOBAYASHI and Y. KUROKAWA, *J. Non-Cryst. Solids* **109** (1989) 164.
15. H. SASAKI, Y. KOBAYASHI, S. MUTO and Y. KUROKAWA, *J. Amer. Ceram. Soc.* **73** (1990) 453.

16. F. SUZUKI, K. ONOZATO and Y. KUROKAWA, *J. Appl. Polym. Sci.* **39** (1990) 371.
17. H. KAWAGUCHI, T. MIYAKAWA, N. TANNO, Y. KOBAYASHI and Y. KUROKAWA, *Jpn. J. Appl. Phys.* **30** (1991) 280.
18. Y. KOBAYASHI, H. SASAKI, S. MUTO, S. YAMAZAKI and Y. KUROKAWA, *Thin Solid Films* **200** (1991) 321.
19. Y. KOBAYASHI, S. NAKATA and Y. KUROKAWA, *Sekiyu Gakkaishi* **34** (1991) 197.
20. Y. KOBAYASHI, S. MUTO, H. SASAKI and Y. KUROKAWA, *J. Surf. Sci. Soc. Jpn.* **12** (1991) 339.
21. Y. KOBAYASHI, S. YAMAZAKI, Y. KUROKAWA, T. MIYAKAWA and H. KAWAGUCHI, *J. Mater. Sci.: Mater. Elec.* **2** (1992) 20.
22. H. OHTA and Y. KUROKAWA, *J. Mater. Sci. Lett.* **11** (1992) 869.
23. Y. KOBAYASHI, S. MUTO, A. MATSUZAKI and Y. KUROKAWA, *Thin Solid Films* **213** (1992) 126.
24. Y. KAKEGAWA, Y. KOBAYASHI, S. MUTO and Y. KUROKAWA, *Nippon Kagaku Kaishi* (1992) 1257.
25. Y. KOBAYASHI, Y. KAKEGAWA, Y. KUROKAWA, K. SUZUKI and Y. OKA, *J. Ceram. Soc. Jpn.* **101** (1993) 69.
26. Y. KUROKAWA, Y. KOBAYASHI and S. NAKATA, *Hetergen. Chem. Rev.* **1** (1994) 309.
27. Y. HOSOYA, S. MUTO, T. OHSUGI and Y. KUROKAWA, *Thin Solid Films* **256** (1995) 4.
28. *Idem.*, *ibid.* **283** (1996) 221.
29. Y. HOSOYA, T. SUGA, T. YANAGAWA and Y. KUROKAWA, *J. Appl. Phys.* **81** (1997) 1475.
30. T. YANAGAWA, Y. KUROKAWA, H. KASAI and H. NAKANHISHI, *Opt. Comm.* **137** (1997) 103.
31. Y. KOBAYASHI, D. KAWASHIMA and A. TOMITA, *Chem. Mater.* **9** (1997) 1887.
32. S. MUTO, T. KUBO, Y. KUROKAWA and K. SUZUKI, *Thin Solid Films* **322** (1998) 233.
33. Y. KUROKAWA, T. SUGA, S. NAKATA, T. IKOMA and S. TERO-KUBOTA, *J. Mater. Sci. Lett.* **17** (1998) 275.
34. Y. KUROKAWA, T. ISHIZAKA, T. IKOMA and S. TERO-KUBOTA, *Chem. Phys. Lett.* **287** (1998) 737.
35. T. ISHIZAKA and Y. KUROKAWA, *J. Appl. Phys.* **90** (2001) 243.
36. *Idem.*, *ibid.* **90** (2001) 2257.
37. *Idem.*, *J. Lumines.* **92** (2001) 57.
38. T. ISHIZAKA, Y. KUROKAWA, T. MAKINO and Y. SEGAWA, *Opt. Mater.* **15** (2001) 293.
39. T. ISHIZAKA, S. MUTO and Y. KUROKAWA, *Opt. Comm.* **190** (2001) 385.
40. T. ISHIZAKA, R. NOZAKI and Y. KUROKAWA, *J. Phys. Chem. Solids* **63** (2002) 613.
41. T. ISHIZAKA, S. TERO-KUBOTA, Y. KUROKAWA and T. IKOMA, *ibid.* **64** (2003) 801.
42. T. ISHIZAKA, Y. KOBAYASHI and Y. KUROKAWA, *J. Mater. Sci.* **38** (2003) 1239.
43. B. E. YOLDAS, *Amer. Ceram. Soc. Bull.* **54** (1975) 286.
44. E. V. BALLOU and T. WYDEVEN, *J. Colloid Interf. Sci.* **41** (1972) 198.
45. A. F. M. LEENAARS and A. K. BURGGRAAF, *J. Membr. Sci.* **24** (1985) 261.
46. B. E. YOLDAS, *J. Non-Cryst. Solids* **147/148** (1992) 614.
47. C. E. JONES and D. EMBREE, *J. Appl. Phys.* **47** (1976) 5365.
48. V. N. BAGRARTASHVIL, V. A. RADTSIG, A. O. RYBALTOVSKII, P. V. CHERNOV, S. S. ALIMPIEV and Y. O. SIMANOVSKII, *J. Non-Cryst. Solids* **180** (1995) 221.
49. G. FU and L. F. NAZAR, *Chem. Mater.* **3** (1991) 602.
50. J. T. KLOPROGGE, D. SEYKENS, J. B. H. JANSEN and J. W. GEUS, *J. Non-Cryst. Solids* **152** (1993) 207.
51. S. ACOSTA, R. J. P. CORIN, D. LECLERCQ, P. LEFÉVRE, P. H. MUTIN and A. VIOU, *ibid.* **170** (1994) 234.
52. G. KUNATH-FANDREI, T. J. BASTOW, J. S. HALL, C. JÄGER and M. E. SMITH, *J. Phys. Chem.* **99** (1995) 15138.
53. M. GUGLIELMI, *J. Sol-Gel Sci. Tech.* **8** (1997) 443.
54. M. SIMÕES, O. B. G. ASSIS and L. A. AVACA, *J. Non-Cryst. Solids* **273** (2000) 159.
55. D. C. L. VASCONCELOS, J. A. N. CARVALHO, M. MANTEL and W. L. VASCONCELOS, *ibid.* **273** (2000) 135.
56. L. CAMPANIELLO, P. BERTHET, F. D'YVOIRE and A. REVCOLEVSCHI, *J. Mater. Res.* **10** (1995) 297.
57. N. ÖZER, J. P. CRONIN, Y.-J. YAO and A. P. TOMSIA, *Solar Energy Mater. Solar Cells* **59** (1999) 355.
58. R. HAUK, G. H. FRISCHAT and K. RUPPERT, *Glastech. Ber. Glass Sci. Technol.* **72** (1999) 386.
59. J. MASALSKI, J. GLUSZEK, J. ZABRESHI, K. NITSCH and P. GLUSZEK, *Thin Solid Films* **349** (1999) 186.
60. H. VAN OLEPHEN, "An Introduction to Clay Colloid Chemistry" (Wiley, New York, 1977).
61. A. R. GREENBERG and I. LAMEL, *J. Polym. Sci. Polym. Chem. Ed.* **15** (1977) 2137.
62. T. HINO, K. MOCHIDA and S. OKUMURA, *Kobunshi Ronbunsyu* **40** (1983) 225.
63. Y. KUROKAWA, *Desalination* **41** (1982) 115.
64. F. SUZUKI, K. ONOZATO, K. HANEDA and Y. KUROKAWA, *Membrane* **9** (1984) 49.
65. K. ONOZATO and Y. KUROKAWA, *Koubunshi Ronbunsyu* **42** (1985) 29.
66. K. ONOZATO, F. SUZUKI, K. HANADA and Y. KUROKAWA, *ibid.* **42** (1985) 219.
67. Y. KUROKAWA and K. HANADA, *J. Polym. Sci. Part* C **25** (1987) 369.
68. J.-I. ISHIYAMA, T. SHIRAKAWA, Y. KUROKAWA, S. IMAIZUMI and S. SAITO, *Nippon Kagaku Kaishi* (1987) 1964.
69. J.-I. ISHIYAMA, T. SHIRAKAWA, Y. KUROKAWA and S. IMAIZUMI, *Angew. Makromol. Chem.* **156** (1988) 179.
70. Y. KUROKAWA, M. NISHIDA, H. SASAKI and Y. KOBAYASHI, *3rd SPSJ Inter. Poly. Conf.* (1990) 147.
71. H. SASAKI, Y. KOBAYASHI and Y. KUROKAWA, *Koubunshi Ronbunsyu* **47** (1990) 935.
72. Y. KUROKAWA and Y. IMAI, *J. Membr. Sci.* **55** (1991) 227.
73. S. YAMAZAKI and Y. KUROKAWA, *Polym. Commun.* **32** (1991) 524.
74. M. NISHIDA, J.-I. ISHIYAMA and Y. KUROKAWA, *React. Polym.* **14** (1991) 205.
75. Y. KUROKAWA, Y. IMAI, Y. SASAKI and T. MAEDA, *Anal. Biochem.* **209** (1993) 247.
76. Y. KUROKAWA and Y. IMAI, *Koubunshi Ronbunsyu* **30** (1993) 451.
77. H. ISHIKAWA, Y. IMAI and Y. KUROKAWA, *Vibrat. Spectr.* **8** (1995) 445.
78. Y. KUROKAWA, *J. Membr. Sci.* **114** (1996) 1.
79. Y. IMAI, Y. KUROKAWA, M. HARA and M. FUKUSHIMA, *Spectrochimica Acta Part* A **53** (1997) 1697.
80. Y. KUROKAWA, Y. IMAI and Y. TAMAI, *The Analyst* **122** (1997) 941.
81. Y. KOBAYASHI, D. KAWASHIMA and A. TOMITA, *Chem. Mater.* **9** (1997) 1887.
82. Y. IMAI, Y. TAMAI and Y. KUROKAWA, *J. Sol-Gel Sci. Tech.* **11** (1998) 273.
83. D. AVNIR, D. LEVY and R. REISFELD, *J. Phys. Chem.* **88** (1984) 5956.
84. D. AVNIR, V. R. KAUFMAN and R. REISFELD, *J. Non-Cryst. Solids* **74** (1985) 396.
85. V. R. KAUFMAN, D. AVNIR, D.-P. ROJANSKI and D. HUPPERT, *ibid.* **99** (1988) 379.
86. T. FUJII, A. ISHII and M. ANPO, *J. Photochem. Photobio. A.: Chem.* **54** (1990) 231.
87. A. MAKISHIMA and T. TANI, *Commun. J. Amer. Ceram. Soc.* **69** (1986) 72.
88. B. S. DUNN and J. I. ZINK, *J. Mater. Chem.* **1** (1991) 903.
89. "Dye Lasers," 2nd ed., edited by F. P. Schafer (Springer, Berlin, 1977).
90. S. MUTO, H. UCHIDA, K. NAKAMURA, C. ITOH and H. INABA, *Trans. Inst. Electron. Commun. Eng. Jpn.* **E69** (1986) 376.
91. R. M. MACFARLANE and R. M. SHELBY, *J. Lumin.* **36** (1987) 179.

92. W. E. MOERNER and W. LENTH, in "Persistent Hole-Burning: Science and Applications," edited by W. E. Moerner (Springer, New York, 1987) Chap. 7 and other chapters therein.
93. A. R. GUTIERREZ, J. FRIEDLICH, D. HAARER and H. WOLFRUM, *IBM J. Res. Develop.* **26** (1982) 198.
94. H. TANAKA, J. TAKAHASHI, J. TSUCHIYA and K. KAWASAKI, *2nd SPSJ Int. Polymer Conf., Tokyo* (Aug. 1986) 130p-1c-18.
95. *Idem.*, *Meeting Jpn. Soc. Appl. Phys.* (Oct. 1986) 218P-29a-ze-9.
96. *Idem.*, *Meeting Chem. Soc. Jpn.* (Oct. 1987) 399p-2A-29.
97. J. FRIEDLICH and D. HAARER, in "Optical Spectroscopy of Glasses," edited by I. Zschokke (Reidel, Dordrecht, 1986) p. 149.
98. T. NISHI, K. ARISHIMA, H. TABEI and H. HIRATSUKA, *Jpn. J. Appl. Phys.* **27** (1988) 225.
99. "Amorphous Solids—Low Temperature Properties," edited by W. A. Phillips (Springer, New York, 1981).
100. R. JANKOWIAK, L. SHU, M. J. KENNY and G. J. SMALL, *J. Lumin.* **36** (1987) 293.
101. J. L. BREDAS, C. ADANT, P. TOCKY and A. PERSOONS, *Chem. Rev.* **94** (1994) 243 and references cited therein.
102. H. L. HAMPSH, J. YANG, G. K. WONG and J. M. TORKELSON, *Polym. Commun.* **30** (1989) 40.
103. S. COOPER and P. K. DUTTA, *J. Phys. Chem.* **94** (1990) 114.
104. L. C. KLEIN, *Annu. Rev. Mater. Sci.* **23** (1993) 437.
105. T. M. CHE, R. V. CORNEY, G. KHANARIAN, R. A. KEOSIUAN and M. BORZO, *J. Non-Cryst. Solids* **102** (1988) 280.
106. D. Y. CHEN, N. OKAMOTO, T. SASAKI, S. TASAKA and R. MATSUSHITA, *IEICE Trans. E* **74** (1991) 946.
107. L. LEDOUX, J. ZYSS, A. MIGUS, J. ETCHEPARE, G. GRILLON and A. ANTONETTI, *Appl. Phys. Lett.* **48** (1986) 1564.
108. S. K. KURTZ, in "Laser Handbook", edited by F. T. Arecchi and E. O. Shulz-Dubois (North-Holland, Amsterdam, 1972) Vol. 1, p. 923.
109. J. JERPHAGOV and S. K. KURTZ, *Phys. Rev. B* **1** (1970) 1739.
110. C. HALVORSON, T. W. HAGLER, D. MOSES, Y. KAO and A. J. HEEGER, *Synth. Met.* **55–57** (1993) 3961.
111. L. BRUS, *J. Phys. Chem.* **90** (1986) 2555.
112. A. I. EKIMOV, A. L. EFROS and A. A. ONUSHCHENKO, *Solid State Commun.* **88** (1993) 947.
113. K. KIMURA, *Z. Phys. D* **11** (1989) 327.
114. A. HENGLEIN, *Chem. Rev.* **89** (1989) 1861.
115. Z. ZHANG, R. C. PATEL, R. KOTHARI, C. P. JOHNSON, S. E. FRIBERG and P. A. AIKENS, *J. Phys. Chem. B* **104** (2000) 1176.
116. G. PANG, S. CHEN, Y. ZHU, O. PALCHIK, Y. KOLTYPIN, A. ZABAN and A. GEDANKEN, *ibid.* **105** (2001) 4647.
117. F. GARCÝA-SANTAMAÝA, V. SALGUEIRIÑO-MACEIRA, C. LÓPEZ and L. M. LIZ-MARZÁN, *Langmuir* **18** (2002) 4519.
118. C. CHEN, T. TAKEZAKO, K. YAMAMOTO, T. SERIZAWA and M. AKASHI, *Colloids Surf. A: Physicochem. Eng. Aspects* **169** (2000) 107.
119. J. N. ARMOR, E. J. CARSON and P. M. ZAMHRI, *Appl. Catal.* **19** (1985) 339.
120. H. HIRAI, Y. NAKAO and N. TOSHIMA, *J. Macromol. Sci.-Chem.* **A12** (1978) 1117.
121. A. UENO, H. SUZUKI and Y. KOTERA, *J. Chem. Soc., Faraday Trans. 1.* **79** (1983) 127.
122. N. FINLAYSON, W. C. BANYAI, E. M. WRIGHT, C. T. SEATON, G. I. STEGMAN, T. J. CULLEN and C. N. IRONSIDE, *Appl. Phys. Lett.* **53** (1988) 1144.
123. L. H. ACIOLI, A. S. L. GOMES and J. R. RIOSLEITE, *ibid.* **53** (1988) 1788.
124. A. NAKAMURA, H. YAMADA and T. TOKIZAKI, *Phys. Rev. B* **40** (1989) 8585.
125. S. C. DAVIS and K. J. KLABUNDE, *Chem. Rev.* **82** (1982) 153.
126. E. J. HEILWEIL and R. M. HOCHSTRASSER, *J. Chem. Phys.* **28** (1985) 4762.
127. G. SCHMID, *Chem. Rev.* **92** (1992) 1709.
128. R. LAMBER, S. WETJEN, G. SCHULTZ-EKLOFF and A. BAALMANN, *J. Phys. C* **99** (1995) 13834.
129. R. H. DOREMU, *J. Chem. Phys.* **40** (1964) 2389.
130. U. KREIBIG and L. GENZEL, *Surf. Sci.* **156** (1985) 678.
131. I. FARBMAN, O. LEV and S. EFRIMA, *J. Chem. Phys.* **96** (1992) 6477.
132. S. UNDERWOOD and P. MULVANEY, *Langmuir* **10** (1994) 3427.
133. L. M. LIZ-MARZÁN, M. GIERSIG and P. MULVANEY, *ibid.* **12** (1996) 4329.
134. H. HÖVEL, S. FRITZ, A. HILGER, U. KREIBIG and M. VOLLMER, *Phys. Rev. B* **48** (1993) 18178.
135. M. XU and M. J. DIGNAM, *J. Chem. Phys.* **96** (1992) 3370.
136. P. ALEMANY, R. S. BOORSE J. M. BURLITCH and R. HOFFMANN, *J. Phys. C* **97** (1993) 8464.
137. S. FEDRIGO, W. HAEBICH and J. BUTTET, *Phys. Rev. B* **47** (1993) 10706.
138. J. TIGGESBÁUMKER, L. KÖLLER, K.-H. M.-BROEL and A. LIEBSCH, *ibid.* A **48** (1993) R1749.
139. V. V. KRESIN, *ibid.* B **51** (1995) 1844.
140. G. COCCO, S. ENZO, G. FAGHERAZZI, L. SCHIFFINI, I. W. BASSI, G. VLAIC, S. GALVAGNO, G. GALVAGNO and G. PARRAVANO, *J. Phys. Chem.* **83** (1979) 2527.
141. K. S. LIANG, W. R. SALANECK and L. A. AKSAY, *Solid State Commun.* **19** (1976) 329.
142. L. OBERLI, R. MONOT, H. J. MATHIEU, D. LANDOLT and J. BUTTET, *Surf. Sci.* **106** (1981) 301.
143. F. HACHE, D. RICARD and C. FLYTZANIS, *J. Opt. Soc. Am. B* **3** (1986) 1647.
144. F. HACHE, D. RICARD, C. FLYTZANIS and U. KREIBIG, *Appl. Phys. A* **47** (1988) 347; G. N. VAN DEN HPVEN, E. SNOEKS, A. POLMAN, J. W. M. VAN UFFELEN, Y. S. OCI and M. K. SMIT, *Appl. Phys. Lett.* **62** (1993) 3065.
145. C. K. RYU, H. CHOI and K. KIM, *ibid.* **66** (1996) 2496.
146. W. XU, S. DAI, L. M. TOTH and G. D. DEL CUL, *J. Non-Cryst. Solids* **194** (1995) 235.
147. M. DEJNEKA, E. SITZER and R. E. RIMAN, *ibid.* **202** (1996) 23.
148. V. C. COSTA, M. J. LOCHHEAD and K. L. BRAY, *Chem. Mater.* **8** (1996) 783.
149. J. JIN, S. SAKIDA, T. YOKO and M. NOGAMI, *J. Non-Cryst. Solids* **262** (2000) 183.
150. A. PATRA, R. REISFELD and H. MINTI, *Mater. Lett.* **37** (1998) 325.
151. T. FUJIYAMA, T. YOKOYAMA, M. HORI and M. SASAKI, *J. Non-Cryst. Solids* **135** (1991) 198.
152. M. YAMAZAKI, Y. YAMAMOTO, S. NAGAHAMA, N. SAWANOBORI, M. MIZUGUCHI and H. HOSONO, *ibid.* **241** (1998) 71.
153. *Idem.*, *J. Phys.: Condens. Matter* **10** (1998) 954.
154. J. QIU, M. KAWASAKI, K. TANAKA, Y. SHIMIZUGAWA and K. HIRAO, *J. Phys. Chem. Solids* **59** (1998) 1521.
155. J. QIU and K. HIRANO, *Solid State Commun.* **106** (1998) 795.

Received 7 September 2003
and accepted 30 June 2004